UNIVERSITÉ DU QUÉBEC À CHICOUTIMI

MÉMOIRE PRÉSENTE À L'UNIVERSITÉ DU QUÉBEC À CHICOUTIMI
COMME EXIGENCE PARTIELLE DE LA MAITRISE EN INGÉNIERIE

Par

ARASH PEYDA

ÉTUDE NUMÉRIQUE ET EXPÉRIMENTALE POUR DÉTERMINER LE CHAMP ÉLECTRIQUE D'APPARITION DES DÉCHARGES COURONNES À L'AIDE DE LA CONFIGURATION D'ÉLECTRODES TIGE-PLAN

NUMERICAL AND EXPERIMENTAL INVESTIGATION TO DETERMINE CORONA INCEPTION ELECTRIC FIELD FOR ROD-PLANE ELECTRODE CONFIGURATION

OCTOBER 2006

Mise en garde/Advice

RÉSUMÉ

En ingénierie de la haute tension, le calcul du champ électrique soumis aux matériaux diélectriques est une procédure fondamentale pour la conception, la maintenance et les besoins de recherche. Dans ce contexte, les chercheurs choisissent généralement une configuration d'électrodes pour simuler le scénario le plus défavorable du point de vue champ. Le système le plus souvent utilisé est la configuration tige - plan, qui produit au bout de l'électrode HT un champ non uniforme très intense. Pour les isolateurs d'extérieur, l'air est le milieu diélectrique. Par conséquent, plusieurs travaux ont été effectués pour comprendre le processus complexe du contournement dans l'air. Les investigations ont étudié ce phénomène complexe pour expliquer le comportement d'une électrode tige de diamètre donné et des distances d'intervalle d'air avec des tensions continues et/ou impulsionnelles.

Le processus du claquage d'un diélectrique peut être divisé en succession de différents phénomènes physiques hautement non linéaires et dépendant des dimensions de la configuration étudiée. À peine quelques recherches ont été effectuées sur les faibles intervalles d'air soumis à une tension alternative, qui représente pourtant le régime permanent d'opération des équipements HT. Les rares investigations qui ont été menées n'ont pas été concluantes sur le calcul du champ électrique maximal analytique et l'effet des variations des paramètres atmosphériques sur les tensions seuil d'apparition des couronnes de streamers.

En utilisant l'approximation hyperboloïde pour résoudre l'équation de Laplace, Coello a obtenue une équation devenue bien connue et qui est généralement utilisée dans les configurations tige -plan pour calculer le champ maximal. Il existe nombre de travaux qui ont basé leurs calculs sur cette équation en utilisant des tensions de type continu ou impulsivement. Une récente investigation a été menée sur la précision de cette formule pour la détermination de la tension seuil d'apparition des couronnes en AC, dans de faibles intervalles d'air, avec deux électrodes tiges. Elle a prouvé qu'il y avait une différence entre les résultats calculés et ceux obtenus expérimentalement.

Alors, des tests de laboratoire étendus et des simulations numériques ont été menés pour un système d'électrodes tige – plan avec de faibles distances d'intervalle d'air pour calculer et analyser le champ électrique maximal au bout de l'électrode hémisphérique HT. Ces investigations ont conduit à l'élaboration d'une équation empirique précise pour ce type de géométrie spécifique. Aussi, des facteurs de non uniformité appropriés ont été déterminés à partir des faisceaux de données. Ils fournissent des résultats raisonnablement précis pour des besoins pratiques en ingénierie.

Des investigations sur l'effet de la pression atmosphérique et de la variation de la température sur la tension seuil d'apparition des couronnes de streamers ont été aussi menées en laboratoire dans les gammes de pression allant de 101.8 kPa à 22.8 kPa et de température allant de - 20°C à 20°C. Des facteurs de correction appropriés, pour la variation des paramètres atmosphériques mentionnés ci-dessus, ont été déterminés à partir des résultats de laboratoire et comparés avec les données expérimentales.

ACKNOWLEDGEMENT

This Master's thesis was conducted within the framework of the Industrial Chair on Atmospheric Icing of Power Network Equipment (CIGÈLE) at the University of Québec at Chicoutimi (UQAC).

After showing my humble gratitude to my creator, I would like to deeply acknowledge my Director Prof. M.Farzaneh for his guidelines and assistance throughout the whole project. Also my Co-director Dr. H, Javadi for always being there and being a sincere devoted academic.

My earnest gratitude goes to Dr. I.Fofana for his illuminating and helpful suggestions, consultations and patience. Last but not least, to my parents Firouz and Mehan who have always been supportive and went beyond my imagination to facilitate my life with their blood and sweat, and dedicating their whole life to me.

I am also very grateful to M. Pierre Camirand and M. Marc-André Perron for their technical support and their excellent facility maintenance and technical assistance.

Finally, thanks to my partner Kylie for her moral support and incredible love and endurance which kept me on track during the course of this programme.

CONTENTS

LIST OF FIGURES

LIST OF TABLES

NOMENCLATURE

2-D	Two Dimensional
3-D	Three Dimensional
A, a	Equation constants
AC	Alternating Current
a_x, ay, az	Unit vectors in direction of the X, Y, Z axes
B	Equation constant
BEM	Boundary Element Method
C, c	Equation constants
C_r	Stabilising Capacitor
CIGÈLE	Industrial Chair on Atmospheric Icing of Power Network Equipment (acronym in French)
CSM	Charge Simulation Method
D	Diameter of Sphere electrode(s)
d	Gap length
DAQ	Data Acquisition Equipment
DP	Dew Point
E	Electric field; Electric strength
E_{incp}	Electric strength at the point of the rod, in a rod-plane gap arrangement, at the point of corona inception
E_{max}	Maximum electric strength

E_{avg}	Average electric strength at the point of corona inception
EM	Electro Magnetic
f	Field form factor(s)
f_{ij}	Field coefficients
FC	Film Corona
FDM	Finite Difference Method
FEM	Finite Element Method
g	Discharge correction factor parameter (IEC)
h	Absolute humidity
HV	High Voltage
IEC	International Electrical Commission
j	Equation constant
$k_1, k_2, k3, k4$	Curve fitting constants
L	Length of rod
LV	Low Voltage
l	Equation constant
m	Correction factor exponent (IEC)
MOM	Method of Moments
n	Equation constant
P	Air Pressure
p	Potential coefficient matrix
P_0	Standard air pressure
P_{amb}	Ambient pressure
$P_{amb(0)}$	Standard ambient pressure

PD	Partial Discharge(s)
PDE	Partial Differential Equation(s)
PS	Streamer corona
q	Column vector of simulation charges
R	Radius of grounded enclosure
r	Radius of the rod tip
R_d	Current limiting resistor
R_m	Resistive measuring arm
R_{m1}	HV arm of the potential divider
R_{m2}	LV resistor of the measuring arm
R_p	Radius of the plane electrode
RH	Relative Humidity
s	Equation constant
T	Air Temperature
T_0	Standard air temperature
T_{amb}	Ambient Temperature
T&D	Transmission & Distribution
V	Applied Voltage
V_0	Sparkover voltage at standard atmospheric condition
V_B	Breakdown voltage
$V_{50\%}$	50% Breakdown voltage
$V_{0,50\%}$	50% Breakdown voltage at standard atmospheric condition
V_{incp}	Corona inception voltage
$V_{incp(0)}$	Corona inception voltage at standard atmospheric condition

w	Air correction factor exponent(IEC)
ξ	Hyperbola defining parameter
η	Point definer parameter in a hyperbola
γ	Field utilization factor
δ	Air density correction factor (IEC)
$\emptyset$	Diameter
∇	Del operator
φ	Potential
ε	Permittivity
ρ_v	Volume charge density

CHAPTER 1

INTRODUCTION

Chapter 1

Introduction

1.1   General

In High Voltage engineering, electric field calculation in any insulating material is one of the most fundamental procedures for design, maintenance, and research purposes. In external insulator types, air is the insulating medium. For this purpose, normally the researchers choose an electrode configuration to simulate and study the breakdown process in the air gaps. Air gaps, also play a major role in the breakdown characteristics of arc propagation and streamer formation on the outdoor insulators subjected to ice build-up in sub-zero climate regions. These air gaps form between the icicles or ice masses that are present on the surface of the insulator.

The most widely used model "electrode configuration" to simulate a very highly non-uniform field distribution to investigate streamer and corona inception is a rod-plane system, which produces very high non-uniform field at the tip of the HV electrode.

1.2   Problem Definition

It should be noted that recently, more research has been carried out to better understand the processes and mechanisms involved in the initiation and propagation of arc on the ice

surface and their adjacent air gaps [1-3].These researches have shown that the radius of an arc root is one of the major factors determining the flashover voltage of the ice surface.

Therefore, to realize the behaviour of the inception of the arc and its transient propagation till complete breakdown it is of outmost importance to find out the maximum electric strength (E_{max}) at the arc tip in an air gap. To investigate this phenomenon, rod-plane air gaps can be employed to simulate the field non-uniformity at the tip of the arc. Study of the relationship between E_{max} and the dimensions of this particular geometry could greatly assist finding the value of maximum electric strength in very close vicinity of the arc tip.

It should be noted that for Rod-plane systems where the electric field distribution is highly non-uniform, it is impossible to obtain or calculate an equation by solving Laplace's equation to find E_{max}. This is due to the non uniform field of this geometry which makes it impossible to be analytically solved. There is specifically one well-known equation obtained by *Coelho* [4] -refer to chapter 2.2.5.1- based on mathematical hyperboloid approximation, commonly used for rod-plane systems to calculate E_{max}.

Lately, an investigation of the accuracy of this equation under AC voltage with actual experimental results for rod-plane electrode configuration (d>>r) in two especial cases (r=0.92mm, r=1.2mm) was carried out in CIGÈLE [5].

It was observed that, the electric field values obtained by using the finite element method " FEM" are very close to those of experimental ones whereas, the calculated E_{incp} by *Coelho*'s equation was not close to these values. The lab tests were conducted at 20°C, 75.2 cmHg and relative humidity "RH" of 24%. This comparison proved that there is a discrepancy between the results obtained by the equation and experimental results for *AC power frequency voltage.*

Since laboratory tests and computer modelling has always been time consuming and requires specific equipment and difficult to perform, derivation of an equation can significantly expedite and facilitate E_{incp} calculation. Not to mention that, the results would be more accurate and realistic.

Furthermore, a high percentage of the past researches have used switching impulse and/or DC voltages on a very limited rod diameter and gap distances.

Scarcely, any research has been done on short air-gaps under AC voltage, which represents steady-state working condition of the equipment. Even these investigations are not conclusive on any analytical maximum electric strength calculation and effect of atmospheric parameter variations on this system. These data are very scattered and do not contribute a lot for calculation of maximum electric strength at corona inception voltage.

Therefore, additional studies were required to obtain a formula to determine E_{incp} for a suitable domain of rod-plane electrode radii and gap distance. This thesis will provide solid computational information for a HV engineer interested in computation of E_{incp} at PD /corona inception point under AC voltage.

1.3   Research Objectives

The aim of this thesis is to:

- Measure the corona inception voltage for hemispherically capped rod-plane electrode configuration at the point of corona inception for a suitable range of radii on short air gap under AC power frequency voltage.

- Perform computer simulation to obtain an empirical equation for field form factors of hemispherically-capped rod-plane gaps and determine the range of applicability.

- Analyse the obtained data to derive a more accurate equation for calculation of E_{incp} and E_{avg}.

- Investigate the effect of atmospheric pressure and temperature variation on the corona inception voltage by laboratory tests and derive correction factors to standard atmospheric conditions set by IEC.

1.4   Methodology

In order to achieve the objectives mentioned in this project a series of laboratory tests and computer simulation were done. Afterwards, the obtained data was scrupulously studied and analysed. Below, is a summary of the steps taken:

- A data acquisition program using LabView DAQ products and software was developed.

- Using the facilities in CIGÈLE, High voltage tests were conducted on the rod-plane electrodes with rod radii of 0.25 mm< r <3.04 mm and gap spacing of 1 cm< d <15 cm. For this purpose special rods and casings were constructed. Also some modifications were applied to the HV equipment terminals and connectors to suit the technical needs.

- After computer simulation of the same geometry range using Coulomb-3D® [42] , regression technique was applied to simulation and experimental results to derive an equation for the calculation of E_{avg} and E_{incp}.

- Using the regression method mentioned above an expression to calculate field form factors was derived from simulation data.

- Utilising the pressure vessel and climate chamber in CIGÈLE HV laboratory, a series of lab tests was carried out to determine the effect of atmospheric parameters on the corona inception voltage. The ambient pressure range was between 22.8 kPa $< P_{amb} <$ 101.8 kPa and the ambient temperature between -20° C $< T_{amb} <$ 21° C.

- By applying the regression technique, conversion factors to standard atmospheric conditions were deduced and compared with the experimental results.

1.5 Applications

The results of this thesis can be extremely useful for a wide range of HV applications, such as:

- Study of the behaviour of the arc inception and its transient propagation in the adjacent air gaps of icicles and ice build-up on outdoor insulators. Also, the study of the effect of water droplets at the tip of the icicles on reduction of the inception of corona discharges.

- Design of outdoor HV equipments and insulators.

- Research on corona and PD "partial discharge" inception and development.

1.5.1 Significance and benefits of the project

- Improvement of the accuracy of maximum electric strength calculation in short air-gaps in proximity to sharp points and edges in HV equipment by a large percentage (for AC voltage).This leads to elimination of unrealistic E_{incp} values employed in HV apparatus design and set-up clearances.

- Contribution to better understanding of the effect of the atmospheric parameters changes on the corona inception voltage "AC" of short air gaps. This applies almost to all of the outdoor HV insulators in T&D industry.

CHAPTER 2

LITERATURE REVIEW

Chapter 2

Literature Review

In this chapter an attempt has been made to conduct an extensive literature review on all previous research and preliminary subjects relevant to this thesis. These investigations enlighten the reader on how far relevant concepts have been researched and what particular fields and topics need further investigation and study.

Extensive literature review was undertaken to grasp the conceptual subjects. These reviews have been delicately briefed and categorised to facilitate a smooth transition from the basics to recent researches.

2.1   Non-uniform Alternating-field Breakdown

Under electrostatic fields, the discussion of breakdown processes in nonuniform geometry has demonstrated the multitude of variables and the shortcomings of any simplifying assumptions for a proper theoretical analysis. Under alternating field, the same arguments apply and the oscillating field seems to complicate matters even further. For

these reasons, and simply for the lack of any general theory, the treatment here will be purely qualitative.

2.1.1 Power Frequency Corona

At the power frequency (50-60 Hz), the critical distance in uniform fields for the ions in atmospheric air is about 1.2 m [6].This means that the space charges produced will have ample time to leave the gap before the field reverses polarity[7]. Such distances are common in energy transmission systems at high voltages with non-uniform field geometries. At small electrode spacings, when the ions have ample time to cross, the partial discharge, called corona, will develop almost exactly as it does under the steady field of the same magnitude. Since the instantaneous voltage under AC applications varies sinusoidaly, the corona mode will follow suit and vary accordingly. Figure (2.1) illustrates the various corona modes that materialise during a cycle as the voltage is increased, for example, across a hemispherically capped rod-plane gap [6].In this diagram capacitive current is omitted.
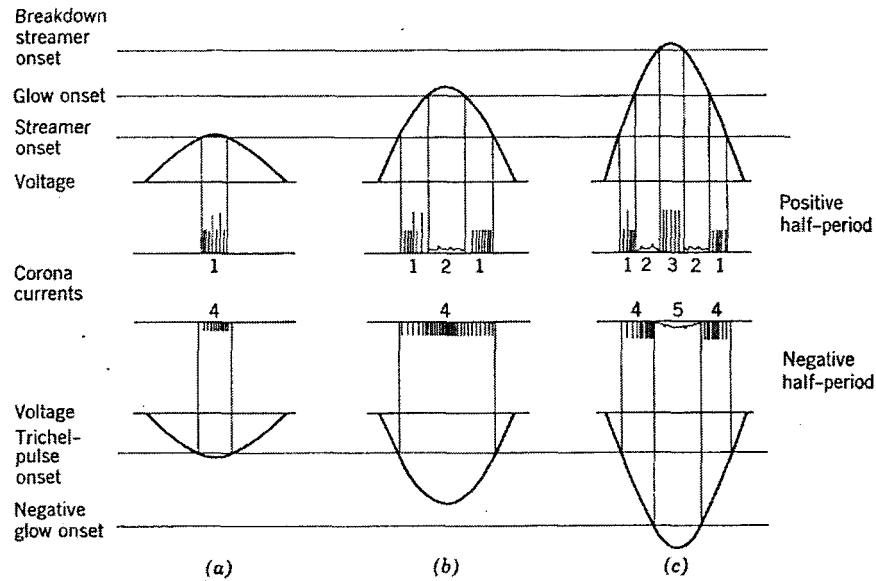
Figure (2.1)   A diagram of the onset current of different positive and negative corona modes at a rod electrode against ground:1.streamers.2.glow.3.breakdown streamers.4.Trichel pulses.5.negative glow [6]

Figure (2.1.a) shows the voltage wave when the peak has just exceeded the anode and cathode corona thresholds which are about the same for both polarities. Hence the first corona modes will develop during both the positive and negative half-periods. Onset streamers are irregular in their sequence, as well as in their amplitude and wave-form, which is hard to define. This behaviour gives rise to the name "burst pulses". In these cases Trichel pulses happen during the negative peak.

About the peak of the negative half-period the highly regular Trichel pulses develop. At very low voltage levels near the onset of corona, and especially if the spacing between the electrodes is well below the critical distance, pulse frequency and magnitude will be the

same during the rising and falling part of the voltage. At very long gaps, the activities will be more pronounced during the first part of each half-period.

When the voltage is raised, its instantaneous value will reach the streamer onset voltage earlier and streamer pulses will be observed, as depicted in figure (2.1.b). The pulse frequency will increase and then decline gradually to zero. If the voltage is high enough, they may be a period about the voltage peak in which no current pulses occure.This is when streamer-glow transition takes place. The glow will then give rise to a continuous but strongly fluctuating current of low magnitude. As the voltage declines, the corona mode will revert to the streamer mode [6].

During the negative half-period, the situation is roughly the same as near the onset, except that here the Trichel pulses frequency will increase. As the voltage is increased further, the onset of breakdown streamers may reach close to the positive peak of the wave. In this case current pulses will develop around the voltage peak, as illustrated in figure (2.1.c) during the negative half-cycle, the onset of the negative glow may be exceeded and a steady current may be observed during the negative peak.

Finally, spark and complete breakdown occurs as the voltage is raised. At standard atmospheric pressure, sparks tend to occur more frequently during the positive half-period [6]. Spark threshold is also lower than that of the negative feathers, and thus will be unable

to materialise in many nonuniform fields. These feathers are hard to detect due to immediate occurrence of breakdown [6].

The most important variable in corona manifestation is the electrode curvature. This curvature together with electrode spacing, will govern the electric field, which determines the length of the streamers and the velocity and time of the drifting of charged particles. Because of the simultaneous occurrence of anode and cathode corona at alternating fields, there are usually two modes of corona that have to be identified. This makes the plotting of such diagrams difficult [6] [8-9]. Figure (2.2) is an example of such a plot for a hemispherically capped rod-plane system of 8mm diameter in atmospheric air [6].The corona inception for a gap spacing of 1 cm$<d<$10 cm is approximately between 15 kV$<V_{incp}<$29 kV. Please refer to the subscript of the figure for description.

125

100

(d)
Spark   8

Peak voltage, kV

75

(c)
Positive glow
and
negative feathers

6

50

(b)
4   3   5

25
2
Streamer
and
Trichel pulses

1

(a)
No ionization

7

0
0   2.5   5.0   7.5   10.0   12.5

d, spacing, cm
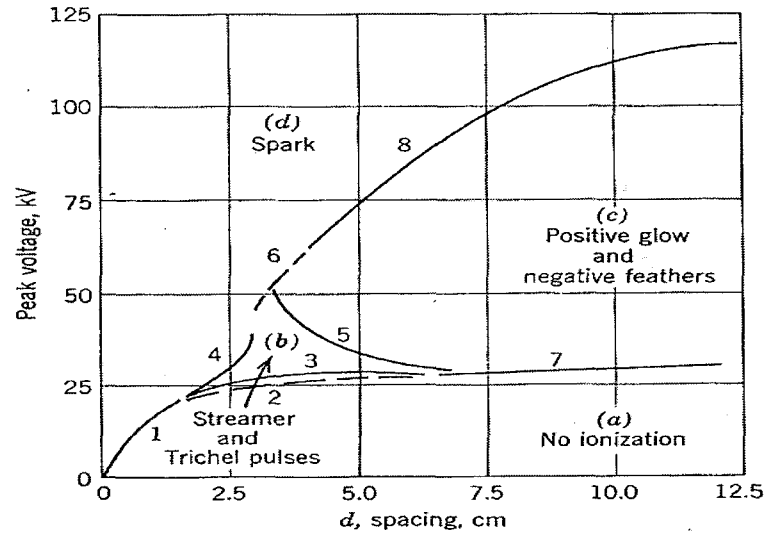
Figure (2.2)   Corona onset and transition voltages of a curvature rod-plane electrode with 4 mm radius. Frequency=50 Hz. Solid curves refer to coronas during the positive polarity, whereas dashed curves describe those for negative polarity.1:spark breakdown with no corona.2:onset of Trichel pulses.3:onset of streamers.4:streamer-spark transition.5:streamer-glow transition.6:negative glow-spark transition.7:onset of positive glow and negative feathers.8:glow-spark transition [6]

2.1.2 Useful Corona Inception Voltage Measurements

Although there is barely any well documented results available for AC corona inception voltage measurement in short air gaps "apart from figure (2.2)", some useful measurements have been noticed for the comparison purpose for this thesis. These experimental results are for positive DC voltage and represent very limited rod-plane gap geometry.

The values recorded by *Isa et al* [9] are presented in figure (2.3).The diameter of the rod is 2 mm and it covers a gap of 1 cm<d<10 cm. The range of the measured DC threshold voltage is approximately between 15 kV<V_{incp}<22 kV. When the gap is smaller than a

critical length, the gap breaks down directly without any corona. However, at gaps larger

than the critical length, breakdown occurs after the appearances of PS "streamer corona"

and FC "Hermestein glow corona or film corona". FC appears at higher voltages than PS.

At the range of the gap length where FC occurs, breakdown voltage increases steeply

compared with that in no-corona region [9].
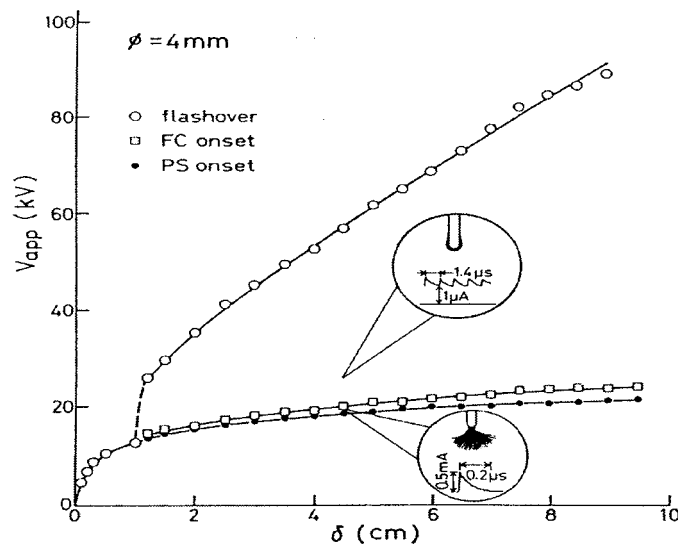
Figure (2.3)   Characteristics of corona inception and breakdown voltages with rod radius
of 2mm. Positive polarity rod-plane gap [9]

Another helpful DC corona inception voltage plot for a rod-plane electrode

arrangement with a 1cm rod radius and a gap range of 1 cm<d<35 cm is depicted in figure

(2.4) [6].For this particular gap arrangement the corona inception voltage starts from 33 kV

up to 56 kV for a gap of 1 cm<d<10 cm.
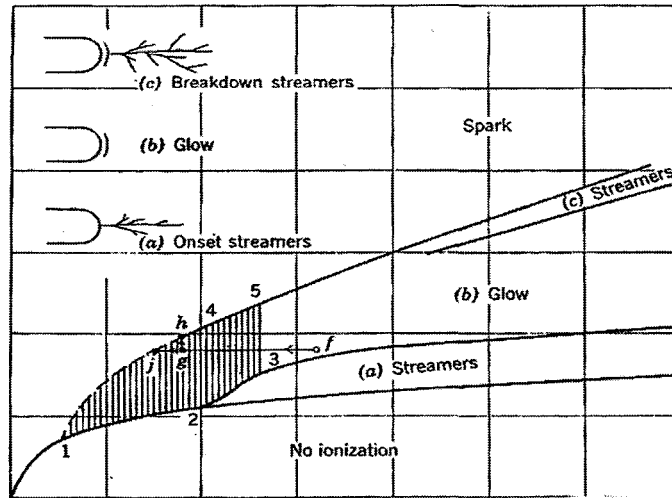
Figure(2.4) Threshold curves for the various modes of anode corona and for spark breakdown for a spherical anode of 1cm radius.1-2 spark threshold;2-3 spark or glow threshold;4-5 glow-spark transition [6]

The last set of results for DC inception voltage measurement is from *Gurumurthy's* [10] experimental results. These results are obtained by using 3 rods with the radii of 1.2mm, 2mm and 3mm for a gap of 1 cm<d<5 cm (figure 2.5).
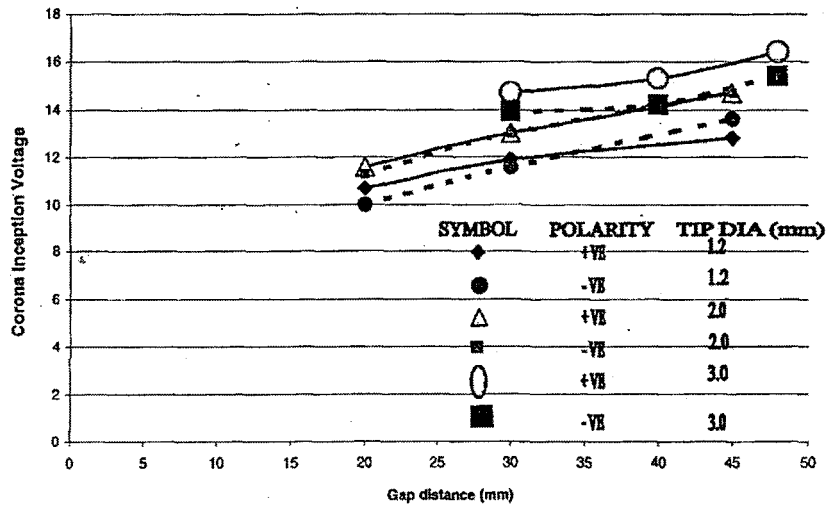
Figure (2.5) Corona inception voltage versus gap distance [10]

The comparison of all these results leads to the conclusion that for the same geometry of a rod-plane system, the DC corona inception voltage is slightly lower than AC corona inception voltage. Although there are some differences between the detected voltages due to test arrangements and conditions plus the detection method for applied DC voltages, by and large, the values of AC corona threshold is more than stable nonuniform fields.

2.2 Electric Field Strength Calculation

2.2.1 Introduction

In HV applications, the dielectric strength of insulating material and the electric field stresses developed in them when subjected to high voltages are the important factors in HV systems. In a high voltage apparatus, the important materials used are, conductors and insulators. While the conductors carry the current, the insulators prevent the flow of the currents in undesired paths. The electric field to which an insulating material is subject to is numerically equal to the voltage gradient given by the following equation,

$$\overline{E} = -\nabla V \tag{2.1}$$

Where E is the electric field vector, V is the applied voltage and ∇ "gradient" operator in Cartesian coordinate system is defined as

$$\nabla \equiv a_x \frac{\partial}{\partial x} + a_y \frac{\partial}{\partial y} + a_z \frac{\partial}{\partial z} \tag{2.2}$$

Where a_x, a_y and a_z are unit vectors in direction of the axes X, Y, Z. The dielectric strength of an insulating material can be defined as the maximum dielectric stress which the material can withstand [11]. The electric breakdown strength of insulating materials depends on a variety of parameters, such as pressure, temperature, humidity, field configuration, nature of applied voltage, imperfections in dielectric materials, material of electrodes and the surface conditions of electrodes, etc [11].

The most common cause of insulation failure is the presence of discharge either within the voids of the insulation or over the surface of the insulation [11]. Failure can occur as a result of thermal or electrochemical deterioration of the insulation. The probability of failure will be greatly reduced if such discharges could be eliminated at the normal working voltage.

Partial discharges are the incomplete failure of insulating materials by discharges which may occur in the internal voids and cavities of the dielectric (solid) or the flashover in air (gas) gaps of insulators due to surface contamination or a follow up of a tracking phenomena (like ice covered insulators) [11]. Also they have a detrimental effect on the power quality and performance of the high voltage apparatus and systems. In practice it is not possible to completely eliminate partial discharges, but a level of PDs is fixed depending on the expected operating life of the equipment. Also, the insulation engineer should attempt to raise the discharge inception level.

It is the intensity of the electric field that determines the onset of pre-breakdown discharges and the rate of increase of current before breakdown. Therefore, it is very essential that the electric strength should be properly estimated and its distribution known in a high voltage equipment. The maximum electric field will normally be at the regions with sharp points which should be alleviated if possible.

2.2.2   Poisson's and Laplace's Equations

Obtaining Poisson's equation is very simple, from the point form of Gauss's law [12],

$$\nabla.\vec{D} = \rho ,$$

$$\vec{D} = \varepsilon\vec{E} , \qquad \blacksquare\!\!\Longrightarrow \qquad \nabla.\vec{D} = \nabla.(\varepsilon\vec{E}) = -\nabla.(\varepsilon\nabla V) = \rho_v$$
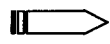
$$\vec{E} = -\nabla V , \qquad\qquad \text{or} \qquad \nabla.\nabla V = -\frac{\rho}{\varepsilon} \qquad\qquad (2.3)$$

Equation (2.3) is Poisson's equation, where the operation $\nabla.\nabla V$ or $\nabla^2 V$ is,

$$\nabla^2 V = \frac{\partial^2 V}{\partial x^2} + \frac{\partial^2 V}{\partial y^2} + \frac{\partial^2 V}{\partial z^2} = -\frac{\rho_v}{\varepsilon} \qquad\qquad (2.4)$$

If $\rho_V = 0$, indicating zero volume charge density, the equation turns to $\nabla^2 V = 0$, which is Laplace's equation.

Laplace's equation is universal for applying as it does wherever volume charge density is zero. It states that every conceivable configuration of electrodes or conductors produces a field for which $\nabla^2 V = 0$. All these fields are different, with different potential values and

different spatial rates of change. So, some certain boundary conditions should be defined in each case to determine the relation of variables in Laplace's equation.

Every problem must contain some known boundary conditions to be solved .These definite equipotential surfaces will provide the boundary conditions for the type of problem to be solved. In other types of cases, the boundary conditions take the form of specified values of E on an enclosing surface, or a mixed of known values of V and E [12].These boundary conditions can be of two types or a combination of these-Dirichlet condition, in which the voltage on the boundaries is known and/or the Neumann condition, in which the gradient at the boundaries is imposed.

Dirichlet condition $\qquad$ $V = V_0$ on boundary $\qquad$ (2.5)

Neumann condition $\qquad$ $E = -\dfrac{\partial V}{\partial n} = C$ n the boundary surface $\quad$ (2.6)

In equations (2.5) and (2.6) V_0 is the prescribed voltage on the boundary surface; n is the outward direction normal to the surface and C is the constant flux given. The insulated, or adiabatic, condition can be obtained by substituting $C=0$.

2.2.3 Analytical Methods

The most satisfactory solution of a field problem is an exact mathematical one. Although in many practical cases such an analytical solution can not be obtained we must resort to numerical approximate solution. Analytical solution is useful in checking solutions obtained from numerical methods.

The most commonly used analytical methods in solving EM-related problems include [13]:

1. separation of variables

2. series expansion

3. conformal mapping

4. integral methods

Since the most powerful analytical method is the separation of variables, this method has been elaborated in this theses and for the rest of the three methods the reader can refer to *Sadiku* [13] for more in-depth explanations. Conformal mapping is restricted to certain EM problems.

2.2.3.1 Separation of Variables

This method (sometimes called the method of Fourier) is a convenient method for solving partial differential equation (PDE). Basically, it entails seeking a solution which breaks up into a product of functions, each of which involves only one of the variables [13]. For example, if we are seeking a solution of a function φ, we require that it has a product form:

$$\varphi(x, y, z, t) = X(x)Y(y)Z(z)T(t) \tag{2.7}$$

To determine whether the method of independent separation of variables can be applied to a given physical problem, one must consider the PDE describing the problem, the shape of the solution region, and the boundary conditions-the three elements that uniquely define a problem [14].

Therefore there are 3 major steps in applying this technique:

1. Separate the (independent) variables.

2. Find particular solution of the separated equations which satisfy some of the boundary conditions.

3. Combine these solutions to satisfy the remaining boundary conditions.

2.2.4   Numerical Methods

2.2.4.1   Finite Difference Method (FDM)

It is rare for real-life EM problems to fall neatly into a class that can be solved by analytical methods. Classical approaches, may fail if:

- The PDE is not linear and can not be linearized without seriously affecting the result.

- The solution region is complex.

- The boundary conditions are of mixed types.

- The boundary conditions are time-dependant.

- The medium is inhomogeneous.

Whenever a problem with such complexity arises, numerical solutions must be employed. From the numerical methods available for solving PDEs, those employing finite differences are more easily understood, more frequently used and more universally applicable then any other.

The finite difference techniques are based upon approximations which permit replacing differential equations by finite difference equations based on Taylor's series approximation. These finite difference approximations are algebraic in form; they relate the value of the dependent variable at a point in the solution region to the values at some neighbouring points. Thus a finite difference solution basically involves three steps:

1. Dividing the solution region into a grid of nodes.

2. Approximating the given differential equation by finite difference equivalent that relates the dependant variable at a point in the solution region to its values at the neighbouring points.

3. Solving the difference equations subject to the prescribed boundary conditions and/or initial conditions.

The most commonly used grid patterns for two-dimensional problems are rectangular grid, skew grid, triangular grid and circular grid [13].

2.2.4.2   Finite Element Method (FEM)

Although the FDM is conceptually simpler and easier to program than the FEM, FEM is a more powerful and versatile numerical technique for handling the problems involving complex geometries and inhomogeneous media. The systematic generality of the method makes it possible to construct general-purpose computer programs for solving wide range of problems.

The finite element analysis of any problem involves basically four steps:

1. Discretisation the solution region into finite numbers of subregions or elements.

2. Deriving governing equations for typical an element.

3. Assembling of all elements in the solution region.

4. Solving the system of equations obtained concerning the Neumann and Dirichlet boundary conditions [13].

2.2.4.3   Charge Simulation Method (CSM)

CSM is one of the basic methods which is widely used and successfully for calculation of electric fields. In this method, the actual electric field is simulated by a number of discrete simulation charges which are located in the conductors and at the interface of the dielectrics. Values of simulation charges are determined by satisfying the boundary conditions at a number of contour points selected at the conductor surfaces. Once the values of simulation charges are determined, then the potential and electric field of any point in the region outside the conductors can be calculated using the superposition principles as follows:

If several discrete charges of any type (point, line or ring) are present in a conductor, the potential at any point at the surface of the conductors and in the region between the conductors can be calculated by the summation of the potential contribution of all the individual simulation charges.

Then, a set of linear equations for the potentials of the contour points can be given by

$$[V] = [p][q] \tag{2.8}$$

Where $[p]$ is the potential coefficient matrix, $[q]$ is a column vector for simulation charges and $[V]$ is a column vector for potentials of contour points.

Electric field strength is calculated by vectorial superposition of magnitudes of various directional components. For example, in Cartesian coordinate system the E_x component of electric field of a point is given by:

$$E_x = \sum_j^n \frac{\partial p_{ij}}{\partial x} q_j = \sum_j^n \left(f_{ij} \right)_x q_j \qquad (2.9)$$

where f_{ij} is a field coefficient at x direction [15-16].

2.2.4.4   Boundary Element Method (BEM)

The Boundary Element Method (BEM) is a numerical method for the solution of boundary value problems. In electrostatics, Maxwell's equations are the governing equations (please refer to equations (2.1) and (2.3)). On interfaces between dielectrics the following condition must be satisfied:

$$\bar{n}.(\overrightarrow{D_1} - \overrightarrow{D_2}) = \rho_S \qquad (2.10)$$

where the normal vector, n , points from medium (2) into medium (1). A scalar electric potential, V, can then be defined as equation (2.1). Using the BEM, material interfaces are replaced with equivalent surface charges and the potential can then be calculated using:

$$V(r) = \frac{1}{\varepsilon_0} \left\{ \int_V G(r,r')[\rho_v(r') + \rho_v'(r')] dv' + \int_S G(r,r')[\rho_s(r') + \rho_s'(r')] ds' \right\} \qquad (2.11)$$

where G is the three-dimensional free space Green's function:

$$G(r,r') = \frac{1}{4\pi} \frac{1}{|r-r'|}$$

(2.12)

ρ_V and ρ'_v are the real and equivalent volume charges respectively in each volume, v ; ρ_s and ρ'_s are the real and equivalent surface charges on each surface s , respectively. The electric field is computed using a similar expression in which the Green's function is replaced with the gradient of the Green's function. In the particular case of electrostatic problems, the BEM has some distinct advantages over methods, such as the Finite Element Method (FEM) and Finite Difference Method (FDM), which use differential operators to compute the field. These advantages include:

- BEM requires only the discretisation of dielectric and conductor surfaces. FEM and FDM require the problem space to be truncated at some arbitrary distance from the model of the device. The entire problem space up to the truncation then requires meshing. The discretisation of only dielectric and conductor surfaces in the BEM reduces user input and storage requirements for the final solution.

- BEM enforces the potential at infinity to be equal to zero. The fields and potentials can then be computed at any point including the interior of devices and the exterior space to infinity. FEM and FDM require an artificial boundary condition to be placed at the truncation of the problem space. This usually requires approximating the

potential to zero or the derivative of the potential to some value at the truncated boundary.

There is an inherent smoothing effect when calculating the fields using integration as opposed to differentiation. Numerical differentiation is much more sensitive to numerical errors in the potential calculation. Smoothing algorithms can be implemented for numerical differentiation but their effectiveness is subject to the basic smoothing operator used [43].

2.2.5   Equations for Calculation of E_{incp} at the Tip of a Rod-plane Gap

2.2.5.1   Hyperboloid Approximation Equation

In order to calculate the electric field in a point-plane gap, *Coelho et al* [4] proposed an equation based on a simple hyperboloid geometric approximation. Based on *Durand*'s parameters and notations the tip is generated by the hyperbola of equations:

$$x = a \sin \xi \cosh \eta$$
$$y = a \cos \xi \sinh \eta$$

(2.13)

Rotating around the x axis depicted in figure (2.6).

Figure (2.6)   Representation of a point-plane configuration with the various quantities involved [4]

Where ζ is the parameter, defining the hyperbola. If $\zeta=0$, it corresponds to Oy axis generating plane and if $\zeta=\pi/2$, ($y=0$), Ox axis generating an infinitely sharp hyperbola. η is the parameter defining a particular point on the hyperbola defined by ζ. a is the distance of the focal point of the hyperbola from the y axis. The value of the electric field at point (ζ, η) is:

$$E(\zeta,\eta) = \frac{C}{a\cos\zeta(\cosh^2\eta - \sin^2\zeta)^{\frac{1}{2}}} \qquad (2.14)$$

Where C is a constant depending on the applied voltage. If we set $\eta=0$, the above equation represents field along the x axis. In this particular case with some approximations, at the tip ($X=0$), we come to:

$$E(0) = \frac{C}{a} = \frac{V}{r \ln\left(2\left(\frac{a}{r}\right)^{\frac{1}{2}}\right)}$$
(2.15)

Assuming $d \approx a$, the electric field strength at the tip of the rod will be [4]:

$$E_{incp} = \frac{2V}{r \ln\left(\frac{4d}{r}\right)}$$
(2.16)

This formula is completely based on mathematical analytical deduction and it assumes that there are no free space charges present between the tip of the rod and the plane. Also, for this equation, no recommended range of rod-plane geometry has been proposed.

2.2.5.2   Empirical Equation (Ice Surface)

Farzaneh & Fofana [2] derived an equation for calculation of E_{incp} at the tip of the hemispherically capped rod at corona inception point, based on experimental and simulation results. The results of this relation are valid for *standard lightning impulse voltage shape 1.2/50 μs on the ice surface*. The tests were carried out on two gap distances of 3.5 and 7cm with 4 rod radii of 1.5, 3, 6 and 9mm, limiting the application range to the mentioned geometric values. The equation is in the form of:

$$E_{inc} = A\exp(B)$$
$$where,$$
$$A = -49\ln(r) + 45; d = 3.5cm$$
$$A = -73\ln(r) + 55; d = 7cm$$

(2.17)

where r is the rod radius in cm and E_{incp} in kV/cm. Naturally, for each gap distance the value of A needs to be recalculated and introduced into equation (2.14). B (in cm μS-1) depends on the HV electrode radii r (cm). The values of the parameter B are relatively small and almost constant. It can be approximated by its mean value of about $8.3 \times 10-4$ cm μS-1.

2.2.5.3   Field Form Factors

From practical point of view, occasionally, the precise solution of field distribution is not always essential for a maintenance or field engineer. This case is applicable to roughly calculate the discharge inception voltage value at the tip of the hemispherically-capped rod-plane electrode. Field non-uniformity factors, f, or their reciprocals, field utilisation factors, γ, have been given in graphical form or in tables by some investigators. Furthermore, some equations based on computer simulation have been obtained by some researchers.

Field factor, f, of an electrode arrangement having nonuniform field is defined as:

$$f = \frac{1}{\gamma} = \frac{E_{max}}{E_{avg}} \qquad (2.18)$$

E_{max} is the maximum of electric field generated around rod electrode and E_{avg} is simply the ratio of corona inception voltage of a rod-plane gap to gap spacing.

2.2.5.3.1   Factors Affecting Field Distribution

It is well known that the field non-uniformity factor of a hemispherically capped rod-plane gap depends primarily on the ratio of the gap length to the radius of curvature of the rod tip [17-18]. However, there are other factors which affect the field factor, i.e. the length L of the rod electrode, the radius R_p of the plane electrode, and the radius R of the grounded enclosure. The effect of L becomes negligible when L/r (radius at the rod tip) is larger than 2.The effect of the grounded enclosure on the field factor becomes insignificant when R/d (gap distance) is larger than 5. Even if these values lie in the error prone area, the effect of the geometries mentioned above are around 1-4% [17].

2.2.5.3.2   Expressions of the Field Factors

There are three sets of the field factors widely used by investigators; the first set is introduced by *Qiu* [17]. These expressions were obtained by using curve-fitting techniques

on the computed data for field factors as a function of *d/r* published by different investigators. As stated by Qiu the accuracy of these expressions is within 5%.

$$f = 0.85(1+\frac{d}{r}); \left(\frac{d}{r} < 3\right)$$

(2.19)

$$f = 0.45\frac{d}{r}\frac{\ln\left(\frac{6d}{r}\right)}{\ln\left(\frac{d}{r}\right)}; \left(3 < \frac{d}{r} < 500\right)$$

The second equation is derived by *Azer et al* [16]:

$$f = 0.6162\left(\frac{d}{r}\right)^{0.9716} + 1.1377; \left(0.8 < \frac{d}{r} < 40\right)$$

(2.20)

And the last relation is reported and utilised by *Stangherlin* [19]:

$$f = 1 + \frac{2}{\frac{r}{d}\left(2+\frac{r}{d}\right)}$$

(2.21)

As investigated by mentioned researchers, the accuracy range of this expression for calculation of E_{max} is case related and depends on the voltage wave shape.

2.3   Atmospheric Correction

2.3.1   IEC Recommendation (Sparkover Voltage)

The disruptive discharge of external insulation depends upon atmospheric conditions. Usually, the disruptive discharge for a given path in air is increased by an increase in either air density or humidity. However, when the relative humidity exceeds about 80% and the disruptive discharge voltage becomes irregular.

By applying correction factors, a disruptive discharge voltage measured in given test conditions, may be converted to the value that would have been obtained under the standard reference atmospheric conditions. Therefore we have,

$$V = V_0 K; where\ K = k_1 k_2 \qquad (2.22)$$

k_1 is the air density correction factor and k_2 is the humidity correction factor. V_0 is the voltage at standard reference atmosphere [20].

2.3.1.1 Air Density Correction Factor

The air density correction factor may be expressed as [20]:

$$k_1 = \delta^m \tag{2.23}$$

When the temperatures T and T_0 are expressed in degrees Celsius and the atmospheric pressures P and P_0 are expressed in the same units (kPa or mbar), the relative air density is [20]:

$$\delta = \left(\frac{P}{P_0}\right)\left(\frac{273 + T_0}{273 + T}\right) \tag{2.24}$$

2.3.1.2 Humidity Correction Factor

The humidity correction factor may be expressed as [20]:

$$k_2 = k^w \tag{2.25}$$

Where k is a parameter depending on the test voltage and may be approximately obtained as a function of the ratio of absolute humidity h, to the relative air density δ, using recommended curves [20]. w, is an exponent defined in next section. This method is valid for values of $h/\delta < 15$ g/m^3.

2.3.1.3 Exponents *m* and *w*

Since the correction factors depend on the type of pre-discharges, this fact is taken into account by parameter *g* defined as [20]:

$$g = \frac{V_{50}}{500L\delta k} \qquad (2.26)$$

V_{50} is the measured 50% disruptive discharge voltage at the actual atmospheric conditions in kV. *L* is the minimum discharge path in meters. The approximate values of *m* and *w* are given in IEC as a graph. The mentioned exponent values have been derived from experimental results obtained in different conditions. However, these are limited to altitudes between sea level and 2000 m.

2.3.2 Effect of Atmospheric Temperature Parameter

The only research on the effect of atmospheric temperature variation on corona inception voltage for a rod-plane gap is carried out by *Allen et al* [21-22]. The rod radius of the geometry is 5mm and gap spacing of 1cm. The gap was tested at varying elevated temperature in the range of 288-494°K under DC voltage. The results are depicted in Figure (2.7).The rate of decrease of V_{incp} in a 206°K temperature rise is 9 kV, which depicts a very slow rate of increase in a very wide range of temperature variation.
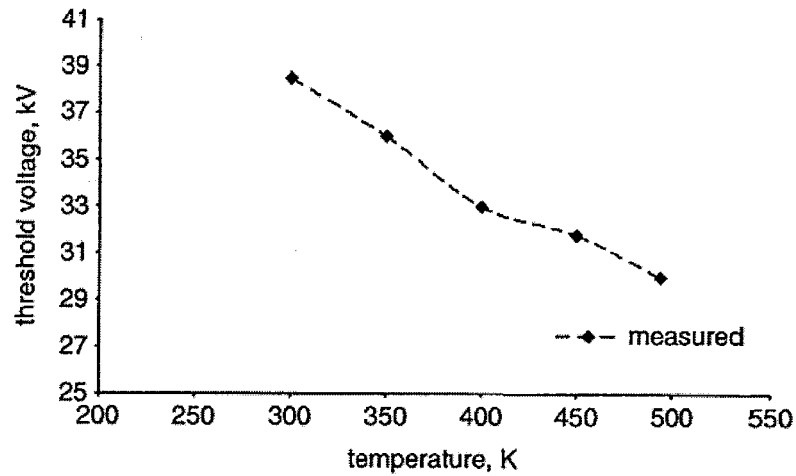
Figure (2.7)   Measured threshold voltage of onset streamer corona as influenced by air temperature [21]

2.3.3   Effect of Atmospheric Pressure Parameter

Shu et al [23] have investigated the relation of *AC 50% breakdown* voltage with low atmospheric pressure at altitudes of 4000 m and above. For this purpose, rod-plane electrode configuration was used with a rod radius of 1mm and gap distances of 10, 19, 26 and 31cm. The results depicted that the 50% AC breakdown voltage is a power function of the pressure, and the characteristic index of the effect of pressure on discharge voltage is related to the type of voltage and gap geometry. Their findings is summarised in figure (2.8).
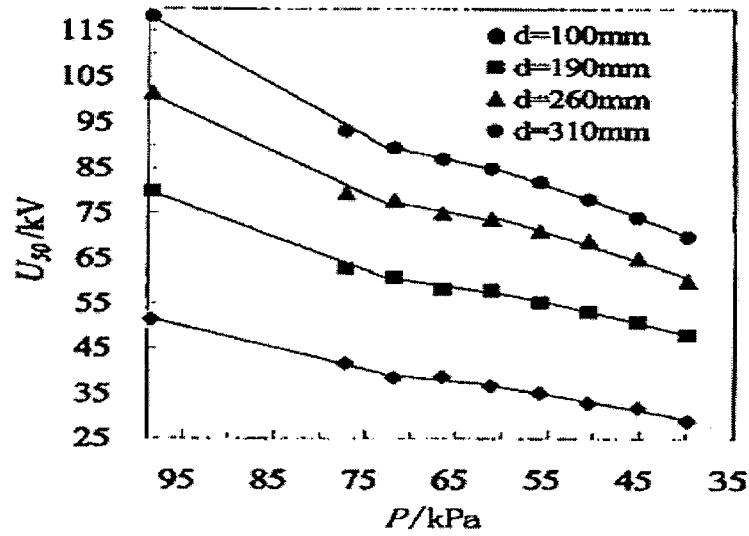
Figure (2.8)   AC discharge voltage U_{50} vs. P [23]

Their proposed correction equation for the effect of atmospheric pressure on AC sparkover voltage is:

$$V_{50} = V_{0,50}\left(\frac{P}{P_0}\right)^{0.4644}$$

(2.27)

2.4   Conclusion & Analysis

Many researches have been conducted to understand the complicated process of breakdown in air-gaps. These researches can be classified under three main categories:

1.   The ones focusing on the physical process of corona and breakdown in the air-gaps, with the aim of probing deeper in understanding the phenomena and explanation of microscopic interactions (electron attachments, photo ionization, velocity of charged

particles,...). Also , their manifestation in the partial and different arc forms and avalanches plus the relation of discharge current to the different contributing voltages[6-9] [14] [24-28]. Most of these researches have used DC or Impulse voltage on medium to long air gaps. Although these studies provide a very good insight for comprehension of the physics of breakdown process, they barely have pointed to any transparent computation technique or equations appropriate for E_{incp}. Nevertheless, they provide some hints for determination of the range of applicability of the derived equation in regards to the dimension of the rod and gap in hemispherically capped rod-plane air gap. Also, these are good references to compare and understand the corona regions of existence in the rod-plane air gaps.

2.   This category mainly hinges on electric field calculation in various electrode configurations. Most of the literature concentrate on numerical computation of electric field using computer modelling such as FEM (finite element method) [13] and CSM (charge simulation method) [15-16] which are irrelevant to the concept of this project and are not able to assist in derivation of a formula nevertheless, good sources for this project's intended computer simulation technique based on FEM. Also there is an expression derived for short air gaps of rod-plane configuration with SF6 insulating medium [29]. The results are validated with numerical values and there is no information about the validity of the results due to voltage shape or with any laboratory tests.

3.   There are a couple of useful empirical formulas for other non-uniform electrode configurations [11] [30] but there is no sign of an equation for calculation of E_{incp} at the tip

of the rod in a rod-plane electrode system. As mentioned in problem definition section, the only equation derived specifically to calculate E_{incp} at the tip of the rod is derived by *Coelho*[4] and has been used in a variety of applications such as research on the corona discharge on ice surface and the adjacent air gaps and propagation of arc on the surface of insulators [1] [3], modelling of discharge in the air gaps [26] [31], arc propagation in the air gaps[26], calculation of the electric strength producing PDs in liquid insulators [32], etc...

For this particular equation, there has not been any mention of applicability or validity in a specific rod and gap spacing range. Therefore, it has been utilised for the rod radius of micro meter up to centimetre range and gap spacing of 0.01 to 1 meter. This almost covers from very short to long air gaps. As it is known from the extensive research on the breakdown process, there are different stages of the development of streamers and partial discharges, each depending on a different set of factors and degrees of contribution to the evolving non-uniformity from the inception of streamer corona to complete breakdown. It is almost impossible to explain the breakdown process generally for all rod-plane gap dimensions, because the streamer build-up process varies among a set of gap and rod radius sizes. Therefore, one should assume that this equation does not fit into all rod-gap size ranges. However, there are some empirical expressions derived to calculate field form factors to estimate an approximation of the values of E_{max}/E_{avg} [16-17] [33] for practical purposes in rod-plane electrode system. The main issue here is that the value of E_{avg} can not be adopted universally as it depends on electrode geometry and the voltage wave-shape applied [6] [10].

Since *Qiu*'s expression for form factors [17] is based on various researchers' results obtained with different rod radius and gap spacing, the applicability of this expression to any gap geometry as long as the gap to rod radius ratio falls into the recommended range is not appropriate. This is due to the fact that there might be different rod-plane arrangements with the same d/r ratio but with different E_{max}/E_{avg} values. Therefore , practically this expression is not substantially useful for research purpose.

Although *Azer et al*'s [16] expression provides accurate values, unfortunately it has a very limited d/r range of applicability (8 <d/r< 40). Thus, making it not useful for the purpose of this thesis's rod-plane arrangements.

The expression cited in *Stangherlin* [19] paper, again, does not mention under what rod-plane arrangement it is derived. In his research with a rod radius of 8mm -rod-plane gap-he has noticed that the accuracy of this expression is valid just for very small d/r ratios.

Although there has been a good correlation of the experimental and calculated results using equation (2.17) for impulse voltage with short gap distances on ice surface [2] within a very narrow geometry range, there has not been any report of the validity of this equation with AC voltage for any range of electrode dimension.

4.   The subject of the last category is generally on the effect of atmospheric parameters variation on the breakdown voltage in rod-plane gaps [18] [22-23] [28] [33-39]. All these studies have demonstrated that the IEC correction method [20] has many setbacks and can not be globally applied to all electrode configurations and voltage shapes. A great majority of these researches have been conducted on medium and/or long air gaps 30 cm-400 cm using DC or Impulse voltages. There are few researches carried out on the effect of humidity in a couple of occasions on 20 cm air-gap showing that there is a large difference between threshold and stability fields for the smaller air gaps [37]. It has been recommended that in the short air gaps (d≤20 cm) the threshold field for streamer propagation in the steady voltage conditions is a good measure to find a factor to replace g in equation (2.21) formula in IEC method, for corona inception voltage [37]. Also the departures from linearity were observed for the smallest gaps.
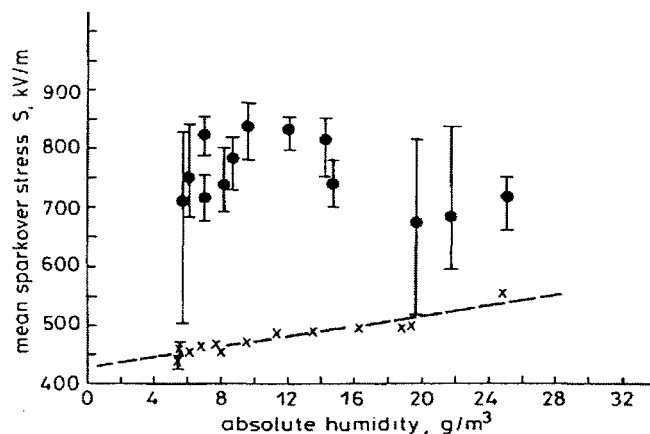
Figure (2.9)   Mean stress for sparkover in the 10 cm gap as a function of humidity,
●: 2mm diameter rod; ×: 20 mm diameter rod [34]

Thus it is clear that conditions at the source of the streamers exert a significant effect on values of the critical ambient fields required for propagation and on the associated humidity coefficient.
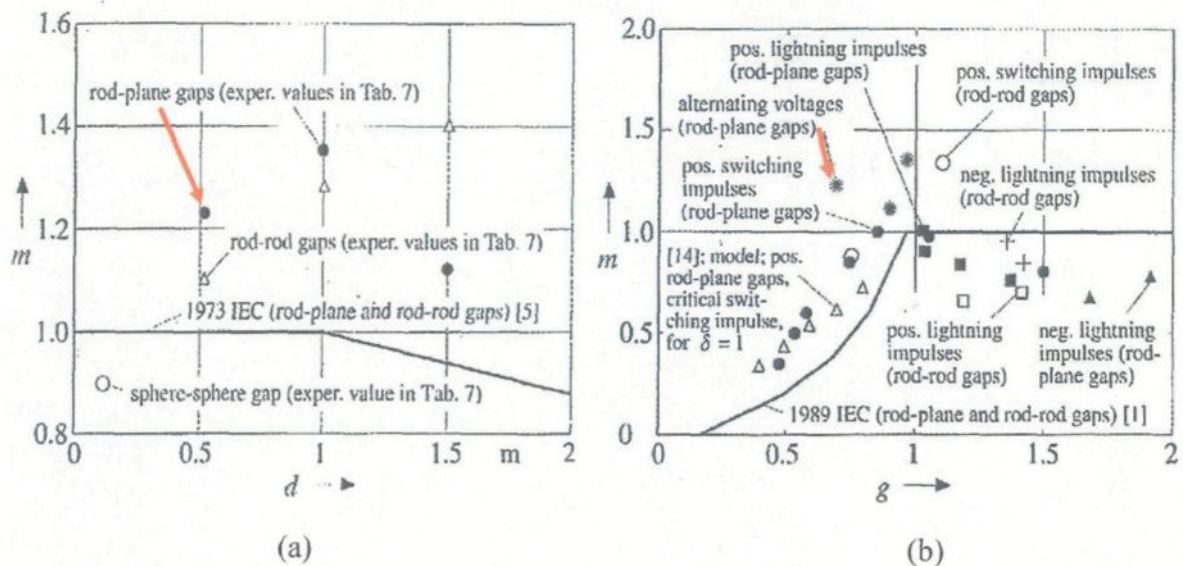
Figure (2.10)   Comparison between the 1989 IEC correction method and published data; (a)Air density exponent m for AC voltage as a function of gap-spacing d for different gaps.(b)Air density exponent m for rod-plane gaps as a function of the density correction factor g [18]

Unfortunately, even in very short gaps (10cm) the measured values of breakdown voltages with different humidity levels have not shown any pattern and mostly scattered, making the determination of g and m values in IEC correction method difficult [34]. Figures (2.9) and (2.10) are some samples of the researches demonstrating the nonlinearity and unpredictability of IEC method in the case of AC voltage and short air gaps.

The problem arises with the fact that the effect of air density seems to be dependent on the combination of air pressure and temperature and the only feasible way to perform the tests is keeping one parameter constant, while varying the other. This leads to different results achieved by different researchers [18]. Not to mention the fact that humidity levels are affected by air temperature as well.

Furthermore, section (2.3.2) proves that more research needs to be done on the effect of temperature variation for the values below room temperature (20 °C) on the AC V_{incp}. Also, all of the results of the research mentioned in section (2.3.3) correspond just to the values above 4000 m and the exponent obtained is suitable for 50% sparkover voltage, emphasising the necessity of investigation on a wider range of atmospheric pressure variation to determine its interaction on AC V_{incp}.

CHAPTER 3

EXPERIMENTAL FACILITIES & TEST PROCEDURES

Chapter 3

Experimental Facilities & Test Procedures

3.1   Experimental Facilities

3.1.1   Introduction

Experimental tests were performed in the high voltage laboratory of CIGÈLE. The high voltage set up was located inside a faraday cage for shielding and standard safety measures. The whole set is comprised of:

1. HV circuit Components.

2. Test and climatic chamber.

3. Pressure Chamber.

4. Atmospheric parameter Measurement kit.

3.1.2   High Voltage Test Circuit & Components

Figure (3.1) represents the schematic diagram of the experimental setup. Figures (3.2) to (3.5) depict the actual set up in the laboratory. A step-up high voltage AC transformer provides the necessary power and voltage to the circuit. The voltage is regulated via a regulating control unit connected to a stabilising capacitor C_r. The circuit is a simple voltage divider with a current limiting resistor R_d and a resistive measuring arm R_m. R_m is a potential divider comprised of two series resistors: R_{m1} and R_{m2}. R_{m1} acts as the HV arm of R_m and R_{m2} is the LV resistor of the measuring arm.

A custom built interconnecting bushing connects the high voltage circuit to the test chamber through the faraday cage. The plane electrode is attached to the common ground wire and leakage current sensing resistance R_c. The voltage and current signals are fed to DAQ Card through a voltage conditioner/limiter. The limiter's cut threshold is ±10 V (peak) . The sampling rate was set to 1000 S/s with a 4000 Hz clock rate. The data is measured and stored by LabView® software. The whole data acquisition system is based on digital sampling which eliminates the noise effect. For the purpose of noise reduction the HV connecting cables were kept as short as possible and at a reasonable clearance from the HV equipment.

The specifications of the high voltage set up are as follows:

- Transformer ratio: $2 \times 220V / 100 - 200$ kV, power: 5 kVA.

- Short circuit capacity: 5-7.5%.

- Measuring arm (resistive) Rm: 100 kV: 140 MΩ.

- Limiting resistance, Rd: 10 MΩ.

- Regulator capacitor, Cr: 0.1 nF.

- Leakage current measuring resistance, R_c: 30 kΩ.
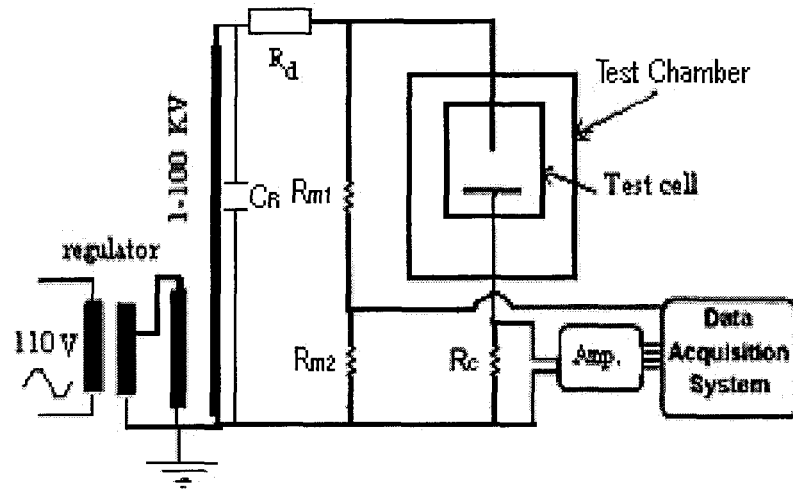
Figure (3.1)   Test circuit diagram

(a)   (b)

Figure (3.2)   (a) Voltage regulator. (b) Regulator capacitor C_r
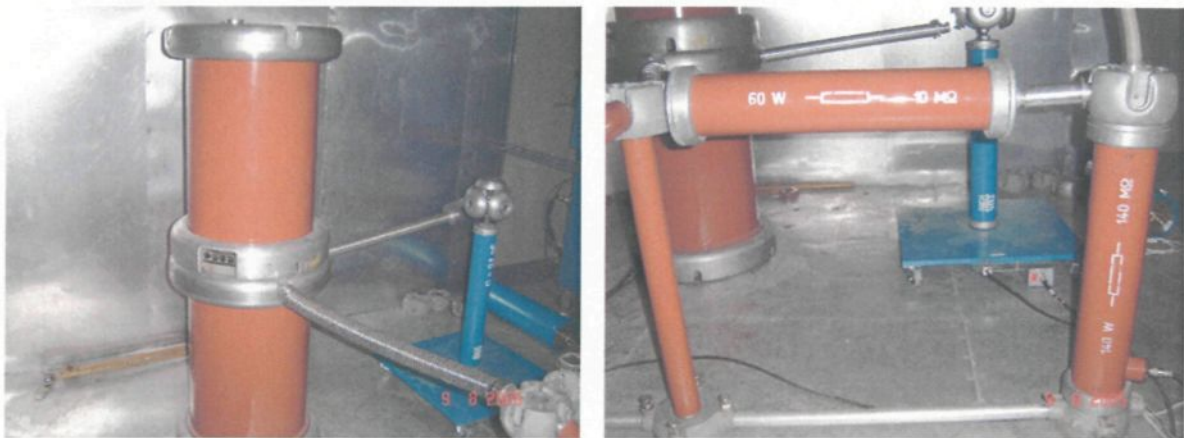
(a)   (b)

Figure (3.3)   (a) High voltage transformer. (b) Limiting resistance R_d and resistive measuring arm R_m

(a)   (b)   (c)
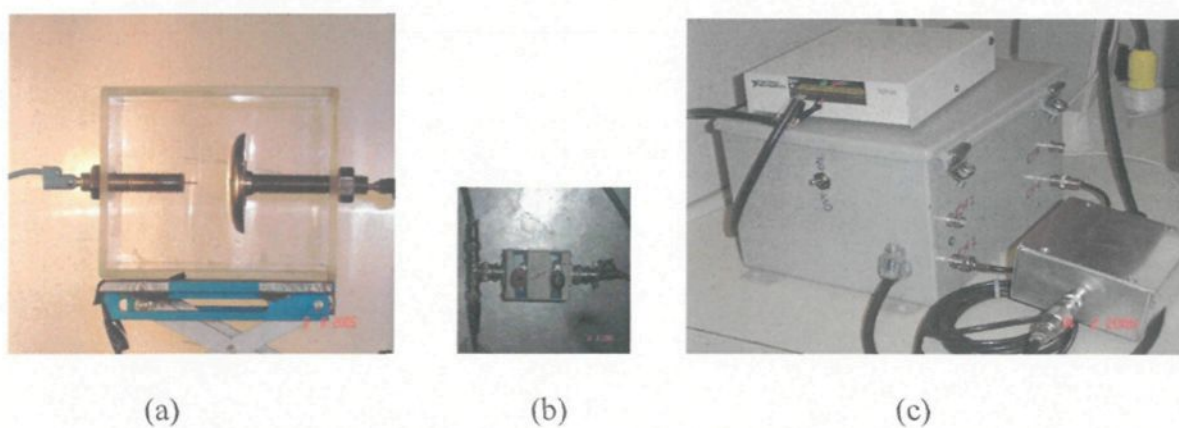
Figure (3.4)   (a) Rod-plane electrodes with adjustable gap spacing, housing. (b) Leakage current measuring resistance R_c. (c) DAQ signal limiter and conditioner
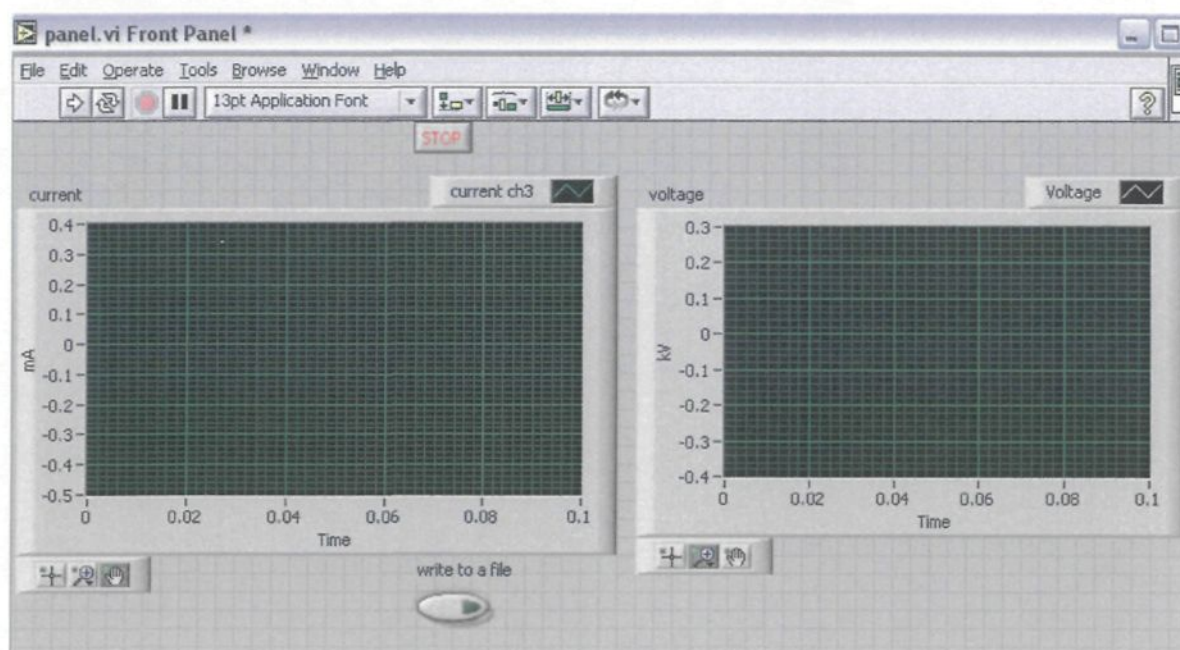
Figure (3.5)   LabView DAQ panel for recording and monitoring voltage and current samples during the tests

3.1.3 Test and Climatic Chamber

The test chamber is a microprocessor based temperature and humidity controller. The chamber is heated through Nichrome wire heating elements and is air cooled with continuous dry nitrogen flow through 100% of the refrigeration system soldering process.

Below is the specification of the climatic chamber:

- **Dimension:** 24"×24"×24".

- **Temperature range:** -73° C to +177° C.

- **Temperature control:** +/- 1.1° C at control sensor.

- **Humidity range:** 20% to 95% RH, +/- 5% RH.

Figure (3.6)   High-low temperature-humidity test chamber

3.1.4   Pressure Chamber

This chamber is a 60 cm×80 cm moulded Plexiglas housing connected to a vacuum pump. This capsule withstands vacuum up to 5 kPa. All the pressure, temperature and humidity sensors were securely placed within the chamber through completely sealed rubber plugs. The slight temperature drops were fine tuned by a 50 W halogen lamp inside the chamber.

Figure (3.7)   Pressure chamber and peripheral measuring equipment

3.1.5   Atmospheric temperature and humidity Measuring Kit

- This kit is a microprocessor-based hygro-thermo anemometer which combines temperature, relative humidity and air velocity measurement..

Figure (3.8)   Atmospheric temperature and humidity Measuring Kit

3.2   Test Procedures

3.2.1   Introduction

To keep the accuracy of corona inception voltage measurement as high as possible, one needs to maintain humidity, air temperature and air pressure nearly constant for each set of tests. Since, it was almost impossible to maintain the atmospheric parameters constant during a whole set of tests "which lasts at least for 4 hours" with high precision, the whole

electrode system was placed inside a test chamber which the atmospheric parameters variations were kept to a minimum and monitored regularly . Yet again, in order to make sure that we gain high precision results, at the start of each test set the breakdown voltage of a standard system (sphere-sphere electrode configuration) was measured. This value would later be employed to convert the obtained corona inception voltages for that particular test set to standard values. In other words, this standard geometry delivers a good reference point for conversion of the obtained values to standard atmospheric condition "T=20°C, P=101.3 kPa and h=11 (g/m^3)".

3.2.2   Procedures for HV Tests

The test steps are described chronologically as follows:

1. At the start of every set of tests the reference point and atmospheric parameters were first measured and recorded. While the tests were carried out, air parameters were constantly monitored and if in any case there was a noticeable deviation from the measured reference point it would be redone to make sure the results were perfectly reliable with minimum error. These recorded parameters were used to convert the obtained data to the standard values.

2. The chosen system for reference is a sphere-sphere electrode configuration with diameters of 10 cm, figure (3.9). These spheres generate an electric field

distribution very close to a uniform one, as the distance between them, d, is adjusted to 1cm and the gap distance between electrodes is less than the diameter of sphere ($\varnothing<2r$). By a combination of the recorded videos with night vision camera and analysis of the recorded voltage and leakage current wave shapes with LabView, it is observed that, for a distance of 1cm at the instant of initiation of the bright spot of corona discharge, breakdown occurs. This confirms that in this particular electrode system, the electric field is completely uniform "in the shortest gap between the spheres" and the maximum value of electric field is equal to the mean.

The peak value of applied voltage at standard condition is 31.8 kV for this specific electrode system therefore, yielding an electric field of 31.8 kV/cm for a gap of 1 cm, which is the minimum required to start corona discharge under test conditions.

Figure (3.9)   Standard sphere-sphere electrode system

3. The rod-plane electrodes are set. The electrodes were made of stainless steel. The plane electrode is a disc with Rogowski profile with a diameter of 8cm. The electrodes were regularly cleaned to remove any dust or particles. Also any possible burnt spots which affect measurement of corona inception voltage caused by flashover arc were completely removed. Care was taken to fasten the electrodes securely to the fixtures of high voltage and earth terminals of the test object to avoid any shock movements as a result of electromechanical forces exerted on electrodes at instant of breakdown.

Figure (3.10) shows the schematic diagram of electrode configuration.
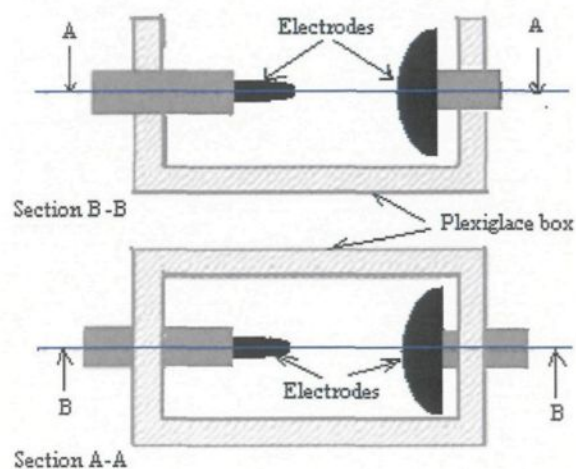
Figure (3.10)   Rod-plane electrode configuration system

- Due to construction difficulty of rod electrodes with radii less than 0.25mm with an acceptable accuracy with the available lathes used in UQAC, the radius

range of rod electrodes was chosen between 0.25 mm $<r<$ 3.04 mm. The gap spacing ranged from 1 cm to 10 cm by 1 cm increments. Additionally, a gap of 15 cm was tested for the whole range of the rods to establish the maximum range of applicability of the derived equation.

- Because of malfunctioning of the interconnecting bushing between the high voltage circuit and the test chamber, the maximum applied voltage was limited to 45 kV rms to avoid any interfering superimposed noise on measured samples.

Figure (3.11) shows the rod electrode set used in rod-plane electrode arrangement.

Figure (3.11)   Hemispherically-capped steel rod electrodes

- Another factor in deciding the radius and gap distance of the measuring system apart from the issues mentioned above is that if we increased the applied voltage above 45 kV rms the partial discharges in the bushing and connecting cable to the test chamber walls would induce high levels of noise on discharge current. Since the magnitude of the current passing through R_c was very small "which made the

corona inception detection a very delicate task", we would have had a very high noise to gain ratio which would affect the measurement accuracy. Due to unquantitative nature of the imposed noise and also varying current signal the noise to gain ratio was practically immeasurable however, the distortion on current wave shape was vividly clear which led to uncertainty in detection of corona inception point.

- According to the tests performed on different insulator types with various wind velocities to obtain an approximate mean value of the icicle radius formed on the insulators [40], the mean radius is 2.5mm which falls into the chosen radius range.

4. Considering the statistic nature of breakdown, for each case, V_{incp} was measured five times and a mean value was recorded. V_{incp} is fairly detectable with partial noise and deformation of current wave shape plus a phase shift from pure capacitive towards pure resistive. This noise-like deformation is actually the envelope of very high frequency small amplitude partial streamers formed around the tip of the rod. In order to find the best means to detect the right time to read the corona inception voltage three traditional methods were checked to figure out the best combination for corona detection.

1. Audio detection

2. Visual detection

3. Current wave shape

It was inspected that because of different sources of audible noise (bushing, high voltage tube connector between the HV circuit and the bushing, connecting cable between the bushing terminal and the HV electrode) this method did not provide an accurate measurement in this case.

For visual inspection in the dark room, it was realised that for gap distances up to 5 cm, since the point of inception and breakdown voltage are very close to each other, this method (which heavily depends upon the eye detection of corona halo plus a very fast reaction to stop the recording at the moment of the inception with a 5 kV/sec rate of rise of the transformer voltage regulator) is not a precise way for detection too. Even for gap distances of 5 cm$<d<$10 cm, application of this method by nature is not able to deliver high accuracy reading due to human error.

To figure out the best way for corona inception voltage detection with available equipment, the breakdown process for the range of the electrode radius for a gap distance of 10cm was recorded with night vision camera. The current and voltage were simultaneously recorded with the voltage rate of rise of 5 kV/sec. The rate of rise of the voltage regulator was the default setting and unadjustable. Since partial discharges show themselves differently on the current waveform for different radius and gap distances of electrodes, all

of these recordings were thoroughly studied to figure out a suitable protocol for corona inception detection by discharge current waveform.

It was noted that the very early voltage irregularities is due to the noise of the connecting cables rather than the audible build up of high electrical stress at the tip of the rod but not yet strong enough to initiate the faint corona glow. Therefore satisfactory measurement accuracy was obtained by combined electrical and visual (camera) recordings of the breakdown process.

- A period of 3 minutes was allowed between each breakdown to eliminate the effect of free space charges and ionised particles within the gap distance.

3.2.2.1   Maximum error percentages due to atmospheric parameters fluctuation

As these variables were recorded during each set of tests the *maximum variation* of these parameters for each set are:

1. Ambient temperature: $4°C \pm 0.2°C$

2. Atmospheric pressure: $0.005 \text{ b} \pm 0.0001 \text{ b}$

3. Humidity: $8\% \pm 2\%$; this humidity change occurred between two extremes of $7.7\text{-}9.24 \text{ gr/m}^3$.

It should be noted that these maximum variations did not occur during the same test set.

3.2.3 Atmospheric Test Procedures

3.2.3.1 Temperature Tests

The procedures described in section (3.2.2) were exactly applied to the tests in climatic chamber. The temperature of the chamber was varied between 20°C and (-20°C) to investigate the effect of low temperatures on V_{incp}. The issues which were needed to be taken care of are detailed as follows:

1. For each electrode arrangement, the value of V_{incp} was measured 7 times and a mean value was calculated . Out of the range values were excluded from the mean inception corona voltage calculation.

2. To avoid formation of frost on the electrode surfaces at sub-zero temperatures, absolute humidity was kept at a constant and low value. Furthermore, the electrodes were regularly cleaned to remove any condensation especially on the surface of the rod tip.

3.2.3.2   Pressure Tests

The procedures described in chapter (3.2.2) were exactly applied to low pressure tests. The Chamber pressure was decreased from 101.8 kPa to 22.8 kPa – this corresponds approximately to an altitude range of 30 m up to 10,500 m- investigate the effect of high altitudes on V_{incp}. Similar to temperature tests, the tests were carried out in low humidity condition and absolute humidity content of the chamber was maintained under (5 gr/m^3) to diminish the effect of humidity on corona inception voltages.

3.3   Conclusion

In this chapter all the equipment specifications have been thouroughly explained. Some alterations were made to the set-up and also care was taken in calibration of the DAQ measurement system to meet the signal sensitivity criteria. Also, the reason for choosing corona detection method has been completely explained. All the test data were stored for subsequent analysis and inspection.

CHAPTER 4

EXPERIMENTAL RESULTS

Chapter 4

Experimental Results

4.1 Introduction

In this chapter, all the results obtained from the laboratory tests are presented. This chapter is divided into 3 sections. The first section represents the measured values of corona inception voltage for derivation of an equation to calculate E_{incp} and E_{avg} at the tip of the rod. The second section, represents the data obtained from atmospheric pressure tests and finally the last section shows the measured values of corona inception voltage due to temperature variation.

4.2 Measured V_{incp} for the Rod-plane Electrode arrangements

After following the test procedures in chapter (3) for the whole geometry range (0.25 mm $<r<$ 3.04 mm and 1 cm $<d<$ 10 cm & 15 cm), leakage current and voltage on the gap was recorded with LabView® software. Since the current wave shape deformities appear differently for different gap geometries, all the waveforms were scrupulously analysed and studied to detect the point of corona/PD-depending on the gap geometry-inception voltage.

Figure (4.1) depicts the detection point of corona inception voltage in a rod-plane electrode arrangement with r=2.48 mm and d=4 cm. Generally, this point is characterised by the slight degree of deformity, an envelope of PDs appearing as noise on the gap leakage current waveform and departure of current phase from pure capacitive towards resistive.
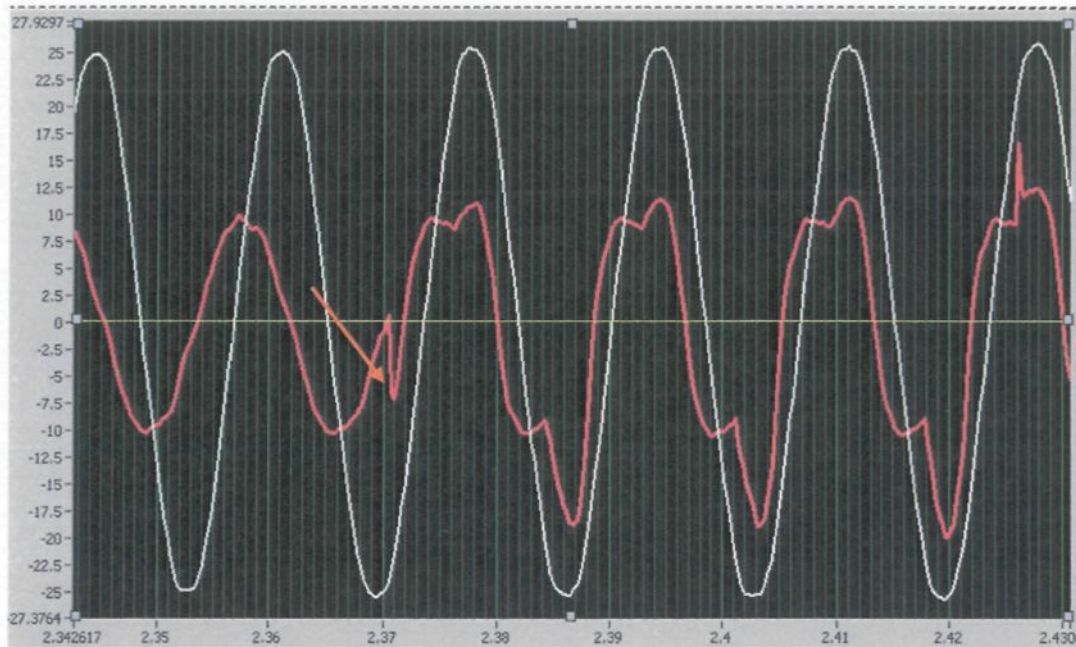
Figure (4.1)   Manifestation of the corona inception on the current wave shape for a rod-plane gap with r=2.48 mm and d=4 cm. Red: gap leakage current in (mA/600), White: gap voltage in kV.

4.2.1   Corona Regions of Existence

- For large diameters of the rod tip, no corona was observed during the whole breakdown phenomena. Instead, the initial ionisation process manifested itself in form of disruptive streamer formations. One of the main reasons is that the transition time from the inception of streamer pulses to complete breakdown is so

short that it is almost impossible to inspect a corona film appearance at the tip of the rod [9].

- For 0.5 mm $<r<$ 2.58 mm & the whole range of gap spacing: at the early stages streamer corona (PS) was developed and later on film corona (FC) appeared.

- For 0.25 mm $<r<$ 0.5 mm & 1 cm $<d<$ 4 cm, there was a very fast transition period from corona to leader development.

- For 0.25 mm $<r<$ 1 mm & 5 cm $<d<$ 15 cm, there was a clear and visible presence of Hermestein corona film on the tip of the rod for a reasonably noticeable period.

4.2.2 V_{incp} Values

Figure (4.2) depicts a plot of the measured V_{incp} for the whole range of radii 0.25 mm $<r<$ 3.04 mm .As one can notice, the plots tend to follow a saturation curve pattern. For $r \leq$ 2.02 mm the magnitude of the error bar percentage is 5%, for $r=2.48$ mm the error bars magnitude is 7% and finally for $r=3.04$ mm the value of the error bars is 8%. The higher value of error in bigger rod radii is due to the difficulty of high accurate detection of the corona inception moment.
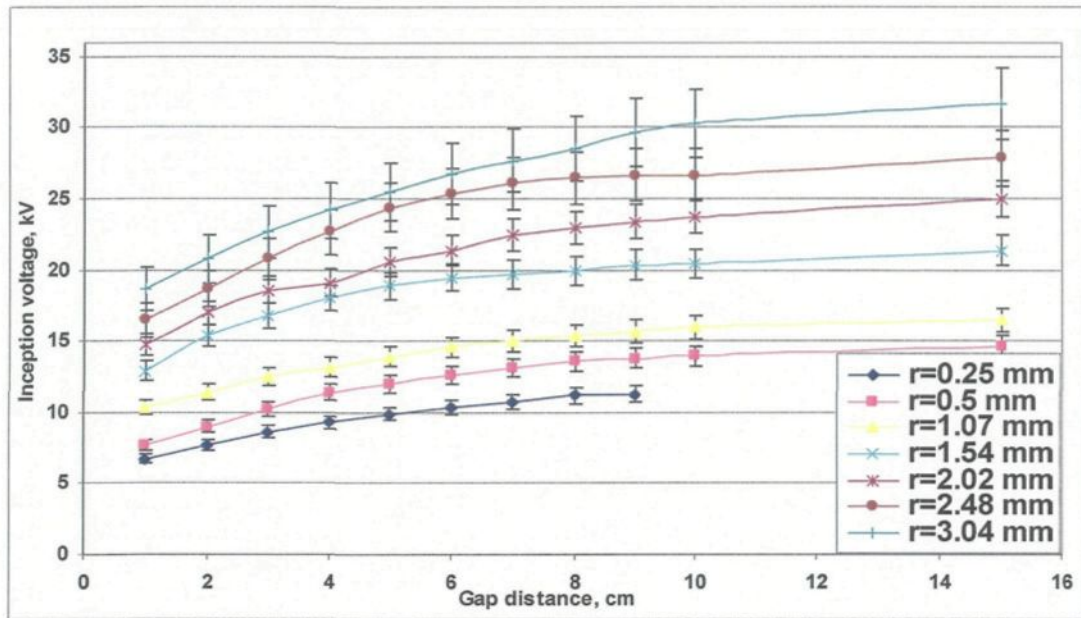
Figure (4.2)   Corona inception voltage of the rod-plane gaps vs. gap spacing

4.3 Atmospheric Temperature Tests

Using the climatic chamber described in chapter (3.1.3) and following the procedure mentioned in sections (3.2.2) and (3.2.3.1), the Measured V_{incp} for a temperature range of, $-20°C < T_{amb} < 20°C$ is plotted in figure (4.3). The chosen geometry for atmospheric tests was set to $r=1.54$ mm and gap of $d=7$ cm to approximately represent the mean value of the experimental set-up geometry. The plot reveals that a temperature decrease from room temperature to $-20°C$ has a relatively slight linear effect on the V_{incp}. For a range of $40°C$ the V_{incp} increase is approximately 3.4 kV.

Figure (4.3)   Effect of ambient temperature reduction on the corona inception voltage for a rod-plane arrangement with r=1.54 mm and d=7 cm. Error bar magnitude: 5%

Table (4.1) represents the test data for temperature tests. The monitored parameters were pressure, temperature, dew point and relative humidity. Absolute humidity was calculated using equation (4.1) [41].

$$h=k(T+q)^{-1}10^{\left(c+\frac{b}{DP+d}\right)}(DP+d)^{a} \tag{4.1}$$

Where h is absolute humidity in kg/m^{3}, T is the ambient temperature in °C, DP is the dew point and a, b, c, q, and k are constants[41]. These constants depend on ambient temperature. If the temperature is sub zero, these constants change. The values for the mentioned constants are summarised in table (4.2) [41].

°C	Air Pressure=101.07 kPa							
	Air Temperature °C							
°C	20	13.7	6.8	0.4	-4	-10	-15	-19.4
V_{incp} (kV)	19.5	20.1	20.6	20.7	21.8	22.5	22.8	22.9
h(gr/m^3)	4.1	3	2.2	1.6	1.1	0.6	0.3	0.3
RH (%)	24	25.4	29.5	32.9	35.4	37	43.6	53
DP (°C)	-1.3	-5.9	-10.1	-14.7	-17.5	-23.5	-24.7	-26.3

Table (4.1)   Monitored ambient parameters during the temperature tests

Equation (4.1) Constants		
	Above Zero	Sub Zero
a	-4.928	-0.323
b	-2937	-2705
c	23.552	11.482
q	273	273
k	0.2167	0.2167

Table (4.2)   Constants for equation (4.1)

4.4 Atmospheric Pressure Tests

Using the pressure chamber described in section (3.1.4) and following the procedure mentioned in sections (3.2.2) and (3.2.3.2), the Measured V_{incp} for an ambient pressure range of 22.8 kPa $<P_{amb}<$ 101.8 kPa-which roughly corresponds to the altitude range of 10,500 m >Altitude>30 m-is plotted in figure (4.4). The diamond points represent the measured values. This plot shows the fact that air pressure variation affects the corona inception voltage more significantly than the ambient temperature variation. For the given pressure range, V_{incp} drops as low as 8 kV for a 22.8 kPa air pressure, which shows a

considerable drop compared to the value of 19.5 kV at 101.8 kPa (the altitude of the laboratory location in Chicoutimi is roughly 30 m above sea level).The chosen geometry for atmospheric tests is the same set used for ambient temperature tests. Table (4.3) provides the monitored ambient parameters during the tests.
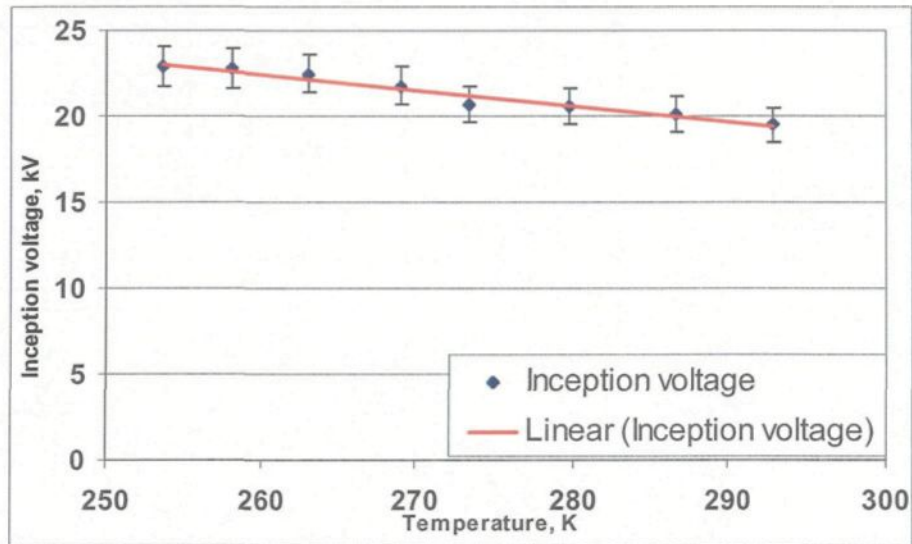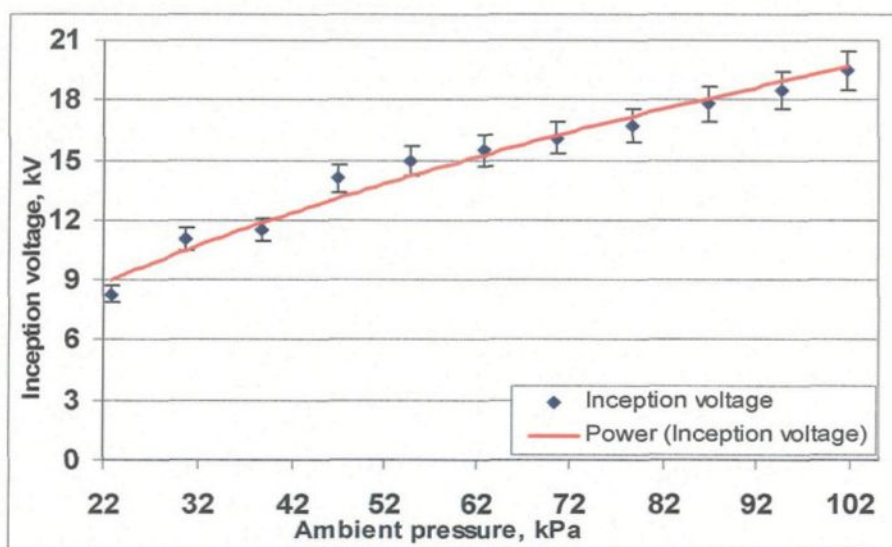

Figure (4.4)   Effect of ambient pressure reduction on the corona inception voltage for a rod-plane arrangement with r=1.54 mm and d=7 cm. Error bar magnitude: 5%

Air Temperature=21°C Air Pressure kPa							
kPa	101.8	94.8	86.8	78.8	70.8	62.8	54.8	46.8
V_{incp} (kV)	19.5	18.5	17.8	16.7	16.1	15.5	15	14.1
h(gr/m^3)	3.42	3.24	3.2	3.06	2.78	2.64	2.53	2.32
RH (%)	18.3	17.2	17.2	16.6	15.9	15.3	14.7	13.7
DP (°C)	-3.7	-4.4	-4.6	-5.2	-5.7	-6.3	-6.8	-7.8

	kPa	38.8	30.8	22.8
	V_{incp} (kV)	11.5	11.1	8.3
	h(gr/m^3)	2.1	1.89	1.9
	RH (%)	12.6	11.5	11.6
	DP (°C)	-8.9	-10.1	-10

Table (4.3)   Monitored ambient parameters during the pressure tests

4.5   Conclusion

In this chapter the values of V_{incp} for all the rod-plane gaps have been presented. Also the observations during the tests have proved that only in rod-plane arrangements with very small radii and gaps wider than approximately 5 cm corona presence in visible. The atmospheric temperature and pressure tests data revealed that for an air temperature drop of -20 °C $<T<$ 20°C, There was an increase of 3.4 kV from standard V_{incp}. Moreover, for the air pressure drop of 22.8 kPa $<P_{amb}<$ 101.8 kPa, a 12.2 kV reduction of V_{incp} from standard atmospheric value was recorded.

CHAPTER 5

COMPUTER SIMULATION

Chapter 5

Computer Simulation

5.1 Introduction

In this chapter, computer simulation of the rod-plane electrodes is discussed thoroughly. Since E_{max} is experimentally difficult to measure in laboratory tests, computer simulation is utilised to determine the form factors for each geometry. These values will be used in computation of E_{incp}.

Simulation was carried out using Coulomb-3D® software which basically uses boundary element method (BEM) to calculate static and quasi-static field problems in a three dimensional medium. The values gained by three dimensional simulations could reach as 4 times higher than the values obtained by real two dimensional simulations for the identical electrode arrangement models.

5.2 Boundary element method (BEM)

There are some hybrid methods which combine FEM and method of moments (MOM) for numerical field analysis and calculations. One of these hybrid methods is BEM. It is a finite element approach for handling exterior problems [13]. It basically involves obtaining the integral equation formulation of the boundary value problem, and solving this by a discretisation procedure similar to that used in regular finite element analysis. Since the BEM is based on the boundary integral equivalent to the governing differential equation, only the surface of the problem domain needs to be modelled. Thus the dimension of the problem is reduced by one as in MOM. For 3-D problems, these elements are taken as triangular elements. Thus the shape or interpolation functions corresponding to sub sectional bases in the MOM are used in the finite element analysis.

5.3 Modelling of Rod-plane Gaps

In computer modelling, the exact replicas of the physical configurations were modelled. The boundary conditions were, 1 V applied to the rod electrode and 0 V to the plane electrode. Depending on the gap distance and radius of the rod, surfaces of the electrodes were discretised with meshing of a refinement degree between 11,000 and 13,000 triangular elements.

Figure (5.1) depicts a 3-D model of a rod-plane gap with r=1.54 mm and d=4 cm, used for atmospheric temperature and pressure tests. Figure (5.2) demonstrates the distribution of electric strength on a profile plane perpendicular to the y axis for the same gap arrangement. In this picture, the magnitude of the electric strength is represented by the colour shades. Hot tones (red, orange, yellow..) represents areas with high values of E whilst the cool shades (green, blue) represent low values. As expected, E_{max} in the air gap is at the tip of the rod, right on the central longitude axis of the rod.
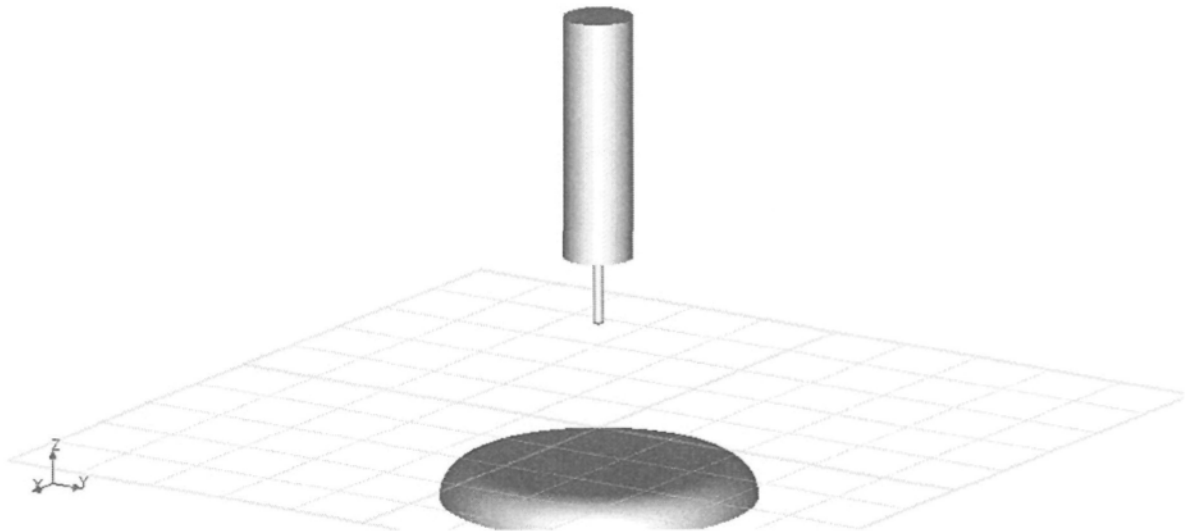
Figure (5.1)   3-D model of a rod-plane gap of r=1.54 mm and d=4 cm
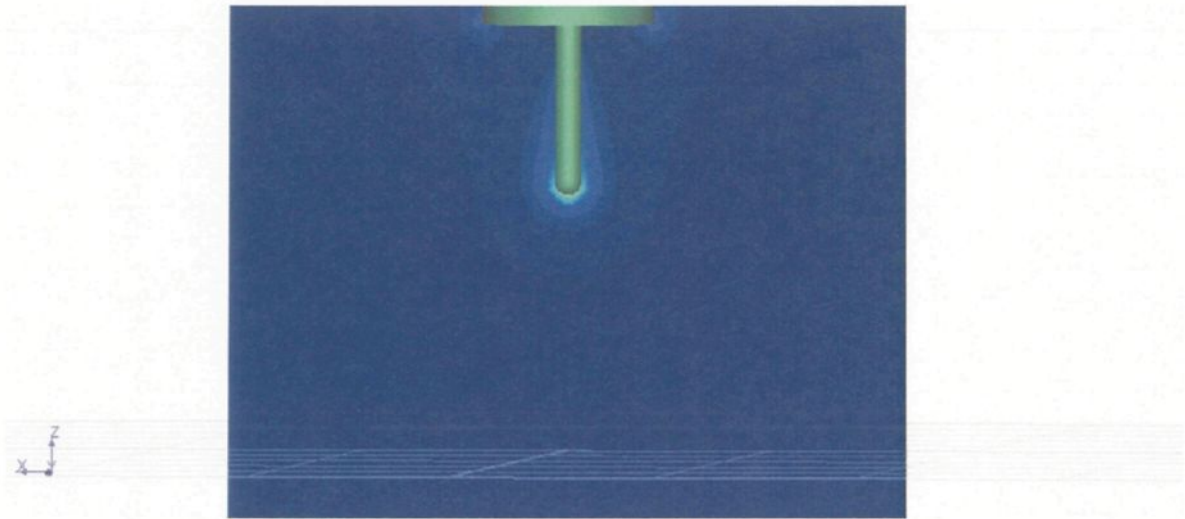
Figure (5.2)   Distribution of electric field in the gap area of an arrangement with r=1.54 mm and d=4 cm

5.4 Simulation Results

Figure (5.3) shows the plots of the simulation results and the values obtained by *Coelho*'s equation. They represent E_{max} at the tip of the rod for a gap distance of 1 cm $<d<$ 10 cm in 1 cm increments and 15cm for an applied voltage of 1 V on the rod. It is evident from the plots that:

- The smaller the radius of the rod and the shorter the gap, the higher is the error of *Coelho*'s equation.

- The maximum error of *Coelho*'s expression occurs at r=0.25 mm and d=1 cm with the value of 9 V/cm. The minimum error occurs at r=3.04 mm and d=15 cm with the value of 0.25 V/cm.

- It appears from the plots that, *Coelho*'s equation provides fairly good results for (r>1.54 mm & d>10 cm).

(a) r=0.25 mm

(b) r=0.5 mm

(d) r=1.07 mm

(d) r=1.54 mm

(e) r=2.02 mm

(f) r=2.48 mm

(g) r=3.04 mm
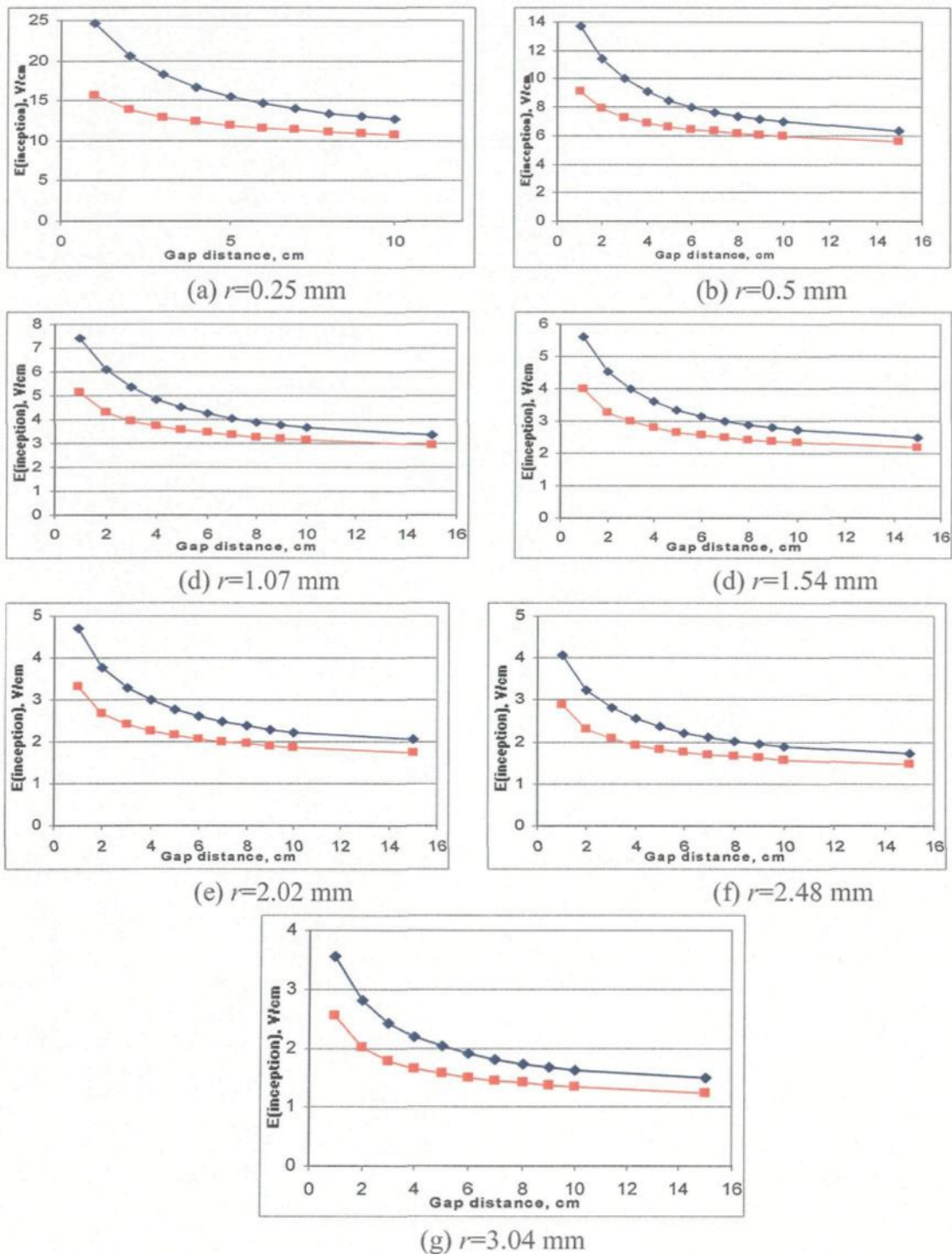
Figure (5.3)   Electrical strength at the tip of the rods vs. gaps for an applied voltage of 1 V on the rod. Blue curves: simulation results; Red curves: Hyperboloid approximation results

5.5 Conclusion

Three dimensional computer simulation of the experimental rod-plane arrangements have shown that hyperboloid approximation equation does return reasonably accurate values in arrangements with $r > 1.54$ mm and $d > 10$ cm "both of these conditions have to be met". Figure (5.3) demonstrates that the smaller the radius of the rod and smaller the gap, the more inaccurate is hyperboloid approximation equation. Simulation results will be later on utilised in derivation of field form factors.

CHAPTER 6

EQUATIONS & DATA ANALYSIS

Chapter 6

Equations & Data Analysis

6.1 Introduction

In this chapter all the test and simulation results have been used to derive equations to calculate f, E_{avg}, E_{incp} for the prescribed range of rod-plane electrode arrangements. Also, correction factors to standard atmospheric conditions for air pressure and temperatures are derived based on experimental results.

6.2 Field Form Factor Expression

Following the completion of computer simulation, using the values of E_{max} and E_{avg}, field form factors were calculated employing equation (2.18). Afterwards, using Matlab's curve fitting tool package, the best fit was applied to the obtained data. The results are demonstrated in figure (6.1). Equation (6.1) is an expression derived from simulation data to calculate form factors for the prescribed gap to radius ratio. In chapter 5 it was elaborately explained that by applying 1 V to the rod electrode and performing computer simulation, the values of E_{max} for all the rod radii and gap distances up to 15 cm were

obtained. Having the applied voltages and gap spacing, E_{avg} is easily calculated using ($E_{avg}=l/d$).Therefore form factors are simply the division of E_{max}/E_{avg}.

$$f = ne^{\left(j\frac{d}{r}\right)} + se^{\left(l\frac{d}{r}\right)}; \left(3 < \frac{d}{r} < 400 \right) \qquad (6.1)$$

where the constants are: $n= 60.79$, $j= 0.001988$, $s= -58.1$, $l= -0.00587$.

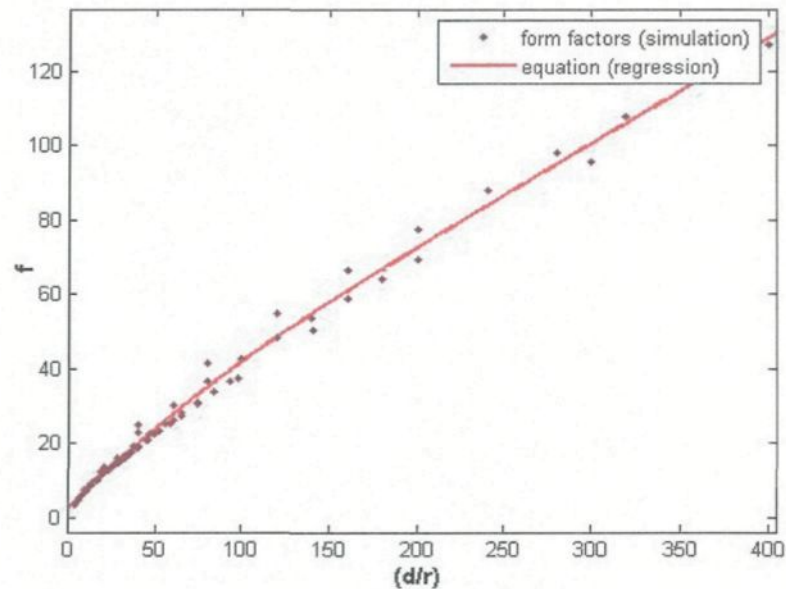

Figure (6.1)   Form factor values obtained by computer simulation. Brown dots: form factors obtained from simulation data using equation (2.18), Red curve: values from derived equation

This equation is valid for very short gaps -max 15 cm- with very small radii up to 3mm and one can not assume that it is universally applicable as long as the d/r ratio falls into the $3 < (d/r) < 400$ range.

6.3   Equation for Mean Electric Strength E_{avg}

Normally for an electrode arrangement which produces uniform field , typically parallel plane, the point of breakdown and corona/partial discharge inception voltage is the same. This occurs around 31 kV/cm in air [14]. Nevertheless, in the case of the electrode arrangements which produce highly non-uniform electric fields in their gap, this value varies considerably. Some factors affecting this value are such as, atmospheric condition, electrode shapes and arrangement and applied voltage waveform [14].

It is very useful for any researcher or engineer to have an expression to calculate the mean electric strength in a rod-plane air gap at the point of the corona/PD inception (AC voltage). This eliminates the availability of test equipment and computer simulation which are expensive and time consuming.

In order to derive an expression, after plotting V_{incp} values obtained by laboratory tests against the gap spacings, regression method was applied to gain the best trendline to all the plots. In this particular case the best fit was found to be of power type:

$$E_{avg} = Ad^{B} \qquad\qquad (6.2)$$

A and B coefficients are fitting constants for each trendline and d is the gap spacing. The second step is to plot constants, A and B, against radii and apply linear regression to A and logarithmic to B as a function of r (rod radius) sets of data in the form of:

$$A = k_1 r + k_2$$
$$B = k_3 \ln(r) + k_4 \tag{6.3}$$

Where, k_1 to k_4 are known coefficients. By substituting A and B values from equations (6.3) with the corresponding values in (6.2), we have:

$$E_{avg} = \frac{4.3103r + 5.8558}{d^{(0.0206\ln(r)+0.781)}} \tag{6.4}$$

In this equation E_{avg} is in kV/cm, r in mm and d in cm. Figure (6.2) demonstrates the plots of equation (6.4) as a function of gap spacing for different rod radii. It also compares the values obtained by equation with the actual experimental ones. These experimental values were simply calculated by dividing V_{incp}/d.
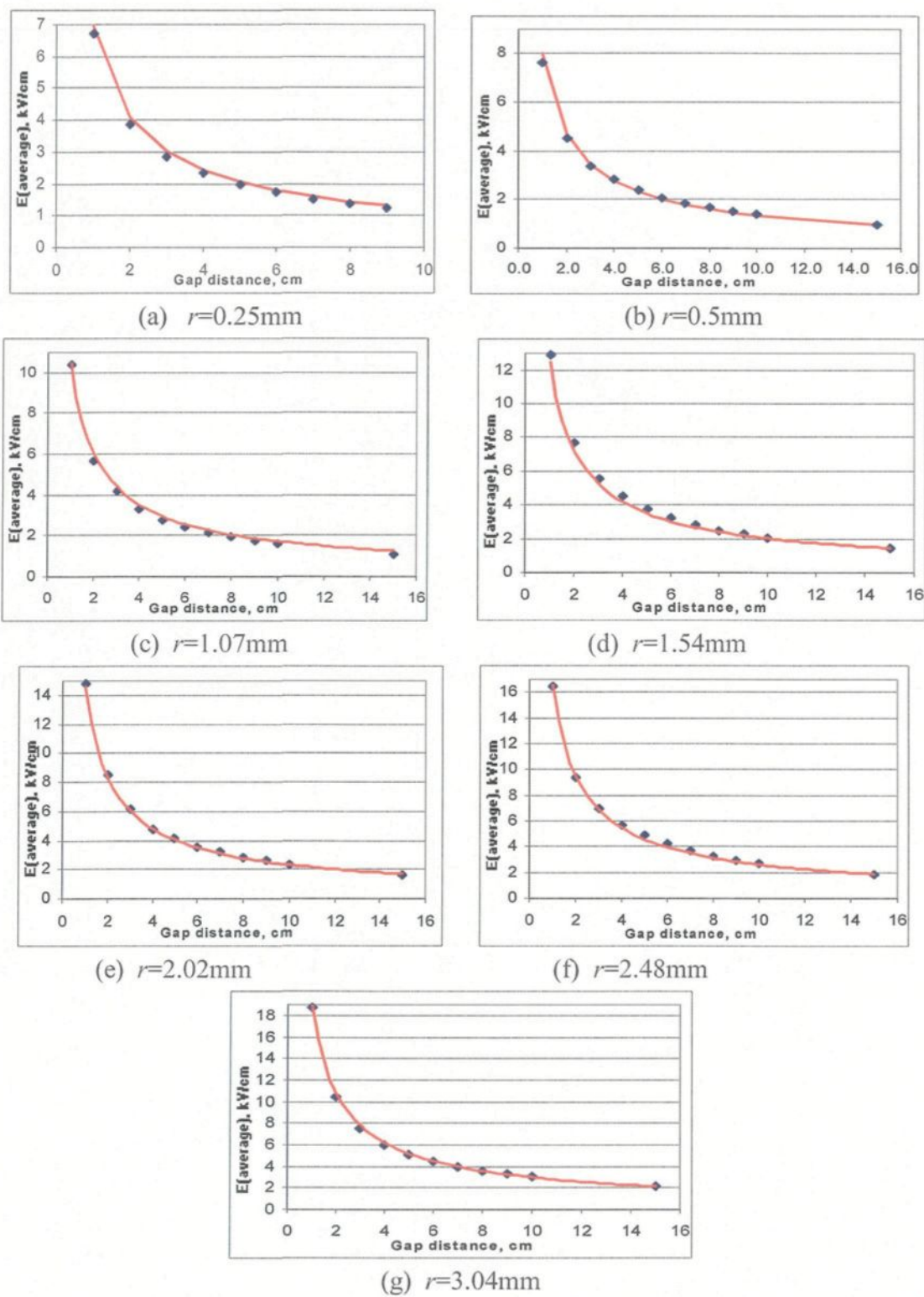
(a) *r*=0.25mm

(b) *r*=0.5mm

(c) *r*=1.07mm

(d) *r*=1.54mm

(e) *r*=2.02mm

(f) *r*=2.48mm

(g) *r*=3.04mm

Figure (6.2) E_{avg} at the corona inception point. Blue diamonds: experimental values; Red curve: derived equation values

Table (6.1) shows maximum and minimum deviation of the derived equation from the experimental values in percentage defined as:

$$Dev = \left| \left(\frac{E_{avg(eqn.)} - E_{avg(exp.)}}{E_{avg(exp.)}} \right) \times 100 \right| \qquad (6.5)$$

Table (6.1) Deviation of Eqn. (6.4) From the Experimental Values in percentage			
	Rod Radius (mm)	Gap (cm)	Deviation
Max	1.07	15	14.09%
Min	3.04	8	0.02%

6.4 Calculation of E_{incp}

The corona onset field strength at the tip of the rod can be calculated from the combination of experimental and computer simulation results. This is achieved by equation (6.6). The first term of the product E_{avg} is derived from experimental results whilst the second term f is deduced from computer simulation.

$$E_{incp} = E_{avg} \times f = \frac{V_{incp} \times f}{d} \qquad (6.6)$$

E_{incp} is in kV/cm, E_{avg} is in kV/cm and f is dimensionless. Having already obtained these values before, E_{incp} is merely the product of these two quantities.

Employing exactly the same procedure for derivation of E_{avg} with the only difference that this time power regression was the best fit for constant A in equation (6.2), equation (6.7) is derived for calculation of maximum electric strength at the tip of the rod at the corona inception point. The range of applicability of this equations is 0.25 mm$<r<$ 3.04 mm and 1 cm$<d<$ 15 cm.

$$E_{incp} = \frac{89.576}{r^{(0.3648)} d^{(0.0349\ln(r)+0.0909)}}$$

(6.7)

E_{incp} is in kV/cm, r is rod radius in mm and d is the gap in cm. Table (6.2) demonstrates the maximum and minimum deviation of the values obtained by equation (6.7) from the results obtained from equation (6.6).

Table (6.2) Deviation of Eqn. (6.7) From Expression (6.6)			
	Rod Radius (mm)	Gap (cm)	Deviation
Max	1.07	15	19%
Min	0.5	8	0.11%

Figures (6.3) and (6.4) depict the results of equation (6.7) and (2.16)-hyperboloid approximation-for the whole range of 0.25 mm$<r<$3.04 mm and 1 cm$<d<$15 cm.

Figure (6.3)   Electric strength at the tip of the rod, at the corona inception point-obtained
by equation (6.7) - vs. gap distance

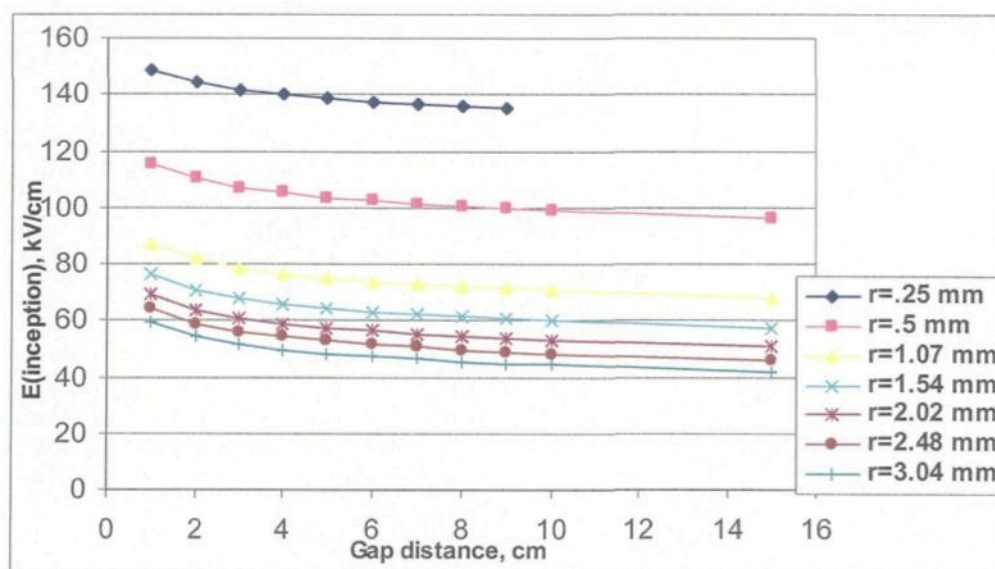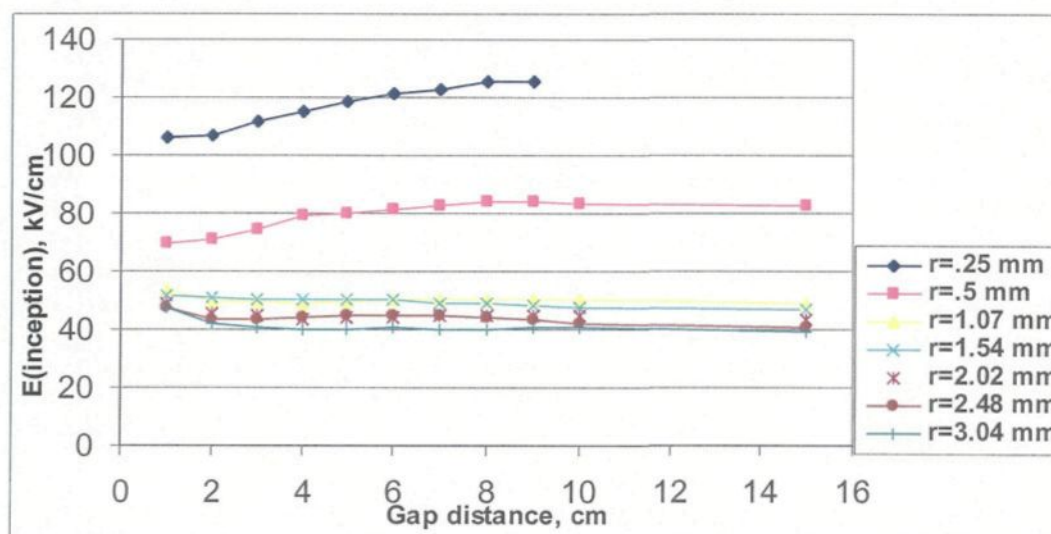Figure (6.4)   Electric strength at the tip of the rod, at the corona inception point-obtained
from equation (2.16) - vs. gap distance

From the above figures, it can be deduced that equation (2.16) returns lower values than

equation (6.7). This difference is quite pronounced for small radii and short gaps. In

addition in figure (6.4), the shape of the rate of decrease of electrical strength at the

inception point for the first three radii of the experimental range is not quite what it is meant to be. This is due to the unrealistic rate of decrease in equation (2.16) which over compensates the values of inception voltage profiles. Going back to figure (4.2), one can see that these profiles can be roughly divided into two sections: the first is for small gaps which have a high rate of rise; the second is after the knee of the curve, for wider air gaps which gradually tends to follow a saturation profile.

6.5   Atmospheric Temperature Correction Factor

Following the discussions in chapter (4.3), in order to achieve a precise correction factor, a power regression method was applied to the data. The result is plotted in figure (6.5). Equation (6.8) represents the graph in analytical form. The maximum error of equation (6.8) in relation to experimental results is 6%.
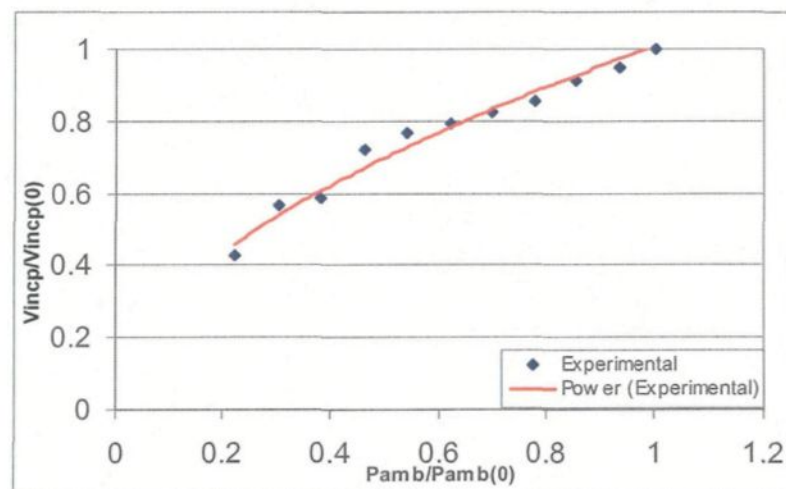

Figure (6.5)   ($V_{incp}/V_{incp(0)}$) vs. (T_0/T) for r=1.54 mm and d=7 cm. T_0=273 °K and $V_{incp(0)}$: 19.5 kV (peak).Blue: Experimental Values; Red: calculated values from equation (6.8)

$$\frac{V_{incp}}{V_{incp(0)}} = 1.09 \left(\frac{T_0}{T} \right)^{1.19} \; ; (253^\circ K < T < 293^\circ K) \tag{6.8}$$

In the above equation, V_{incp} stands for corona inception voltage at temperature T in kV (peak).$V_{incp(0)}$ represents inception voltage at the atmospheric standard condition and T_0 is standard atmospheric temperature which is 20ºC or 293ºK.

6.6 Atmospheric Pressure Correction Factor

Using the obtained experimental data as explained in chapter (4.4), in order to deduce a correction factor, a power regression was applied to the ($V_{incp}/V_{incp\,(0)}$) ratio as a function of ($P_{amb}/P_{amb\,(0)}$) ratio data sets. The obtained results are demonstrated in figure (6.6).Equation (6.9) is the analytical form for calculation of V_{incp} corrected to standard conditions.
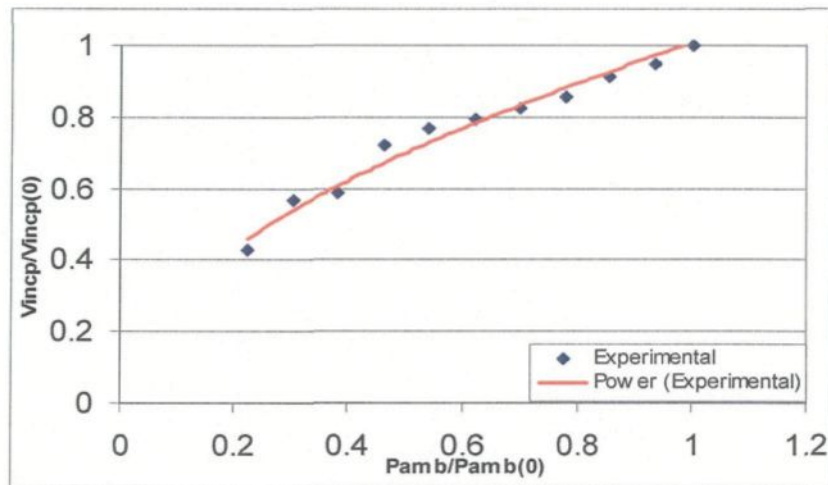

Figure (6.6)   ($V_{incp}/V_{incp(0)}$) vs. ($P_{amb}/P_{amb(0)}$) for r=1.54 mm and d=7 cm. $P_{amb(0)}$=101.3 kPa and $V_{incp(0)}$=19.5 kV (peak). Blue: Experimental Values; Red: calculated values from equation (6.9)

$$\frac{V_{incp}}{V_{incp(0)}} = \left(\frac{P_{amb}}{P_{amb(0)}}\right)^{0.5239} ;\left(22.8kPa < P_{amb} < 101.8kPa\right) \tag{6.9}$$

Where V_{incp} stands for corona inception voltage at ambient pressure, P_{amb}, in kV (peak). $V_{incp(0)}$ represents inception voltage at the atmospheric standard condition and $P_{amb(0)}$ is standard atmospheric pressure with the value of 101.3 kPa.

6.7 Conclusion

All the experimental and simulation results were employed to derive empirical equations to calculate field form factors, maximum and mean electric strength at the point of corona inception for AC applied voltage in short rod-plane gaps. In these equations the only parameters needed are rod radius and gap distance. This fact eliminates the need for V_{incp} values which require elaborate laboratory facilities to obtain. In addition, correction factors were extracted from laboratory tests to correct the effect of ambient temperature and pressure variation on V_{incp}.

CHAPTER 7

CONCLUSIONS AND RECOMMENDATIONS

Chapter 7

Conclusions and Recommendations

7.1 Conclusions

Utilising a rod-plane electrode configuration with a radius range of 0.25 mm $<r<$ 3.04 mm and gap spacing range of 1 cm $<d<$ 15 cm, a series of tests were conducted to measure the corona inception voltage. Computer simulation of the experimental set up was carried out to obtain field form factors. Also, the effect of atmospheric pressure and temperature was investigated on an electrode configuration of $r=$1.54 mm and $d=$7 cm with an air temperature variation range of -20°C $<T_{amb}<$ 20°C and ambient pressure variation range of 22.8 kPa $<P_{amb}<$ 101.8 kPa.

Empirical equations were derived from experimental and simulation results to calculate E_{avg}, f, E_{incp}. Moreover, correction factors for atmospheric parameters were deduced from experimental results. The results and observations are broken down as follows:

1. For large diameters of the rod tip, no corona is observed during the whole breakdown phenomena. One of the main reasons is that the transition time from the

inception of streamer pulses to complete breakdown is so short that with the technique utilised in this study, it is almost impossible to inspect a corona film appearance at the tip of the rod.

2. For 1.5 mm $<\emptyset<$ 4.5 mm and the whole range of gap spacing, at the early stages streamer corona (PS) is developed and later on film corona (FC) appears. For 0.5 mm $<\emptyset<$ 1.5 mm and 1 cm $<d<$ 4cm, there is a very fast transition period from corona to leader development. For 0.5 mm $<\emptyset<$ 1.5 mm and 5 cm $<d<$ 15 cm, there is a clear and visible presence of Hermestein corona film on the tip of the rod for a reasonably noticeable period.

3. For the experimental electrode set up, minimum and maximum measured V_{incp} values are 6.7 kV (peak) and 31.8 kV (peak). The rate of increase profile of V_{incp} follows a saturation curve pattern with steeper rise angle in shorter gaps. This rise angle appears to decrease gradually as radius and gap of the rod-plane electrodes increase.

4. At standard atmospheric pressure, 101.3 kPa, a 40°C decrease of ambient temperature causes an increase of the V_{incp} of 3.4 kV in a rod-plane gap with r=1.54 mm and d=7 cm. This demonstrates that temperature drop does not convey an effect as significant as pressure drop for the same rod-plane geometry. Based on Experimental values, equation (6.8) is empirically derived as a correction factor to calculate V_{incp} for the mentioned temperature variation range.

5. At room temperature, 21°C, a pressure drop down to 22.8 kPa which approximately equals to the air pressure in 10,500 m altitude, reduces the V_{incp} from 19.5 kV to 8.3 kV. Equation (6.9) is derived to calculate the correct the measured values to standard atmospheric condition values.

6. Computer simulation results reveal that equation (2.16) returns very low values of E_{max} particularly in rod-plane electrodes with $r<1.5$ mm and $d=4$ cm. The maximum error of *Coelho*'s expression occurs at $r=0.25$ mm and $d=1$ cm with the value of 9 V/cm. The minimum error occurs at $r=3.04$ mm and $d=15$ cm with the value of 0.25 V/cm. It appears from the simulation results that *Coelho*'s equation returns fairly good results for the rod-plane electrodes with rod radii bigger than 1.54 mm & $d>10$ cm.

7. An empirical expression -equation (6.1) - for calculation of field form factors of the experimental set-up was derived. This equation is only valid for $3< (d/r) <400$ within the prescribed electrode arrangements. The figures show that for this particular range, these values reach up to 125 for $(d/r) = 400$.

8. Based on experimental results, equation (6.4) can be used to calculate E_{avg} for the set up electrode arrangements when the applied voltage is V_{incp}. This expression has a maximum error of 14%.

9. Finally, equation (6.7) was derived from the combination of experimental and simulation results to calculate E_{incp} at the tip of the rod in a rod-plane gap. This equation provides accurate and realistic results which can replace the role of the equation (2.11) for the prescribed rod-plane geometry ranges.

7.2   Recommendations

1. Further studies are needed to investigate the possibility of deriving a formula for form factors and electric strength at the tip of the rod in a medium range gap spacing at the point of corona inception. For this purpose a more sensitive corona detection technique with more sophisticated equipment such as a corona camera, needs to be employed.

2. Since there has not been many researches on the effect of atmospheric parameters on V_{incp}, study of the combined effect of air pressure and temperature on the corona inception voltage in short air gaps is suggested. Also, investigation of the effect of air humidity content on these values can provide useful information for engineering purposes.

REFERENCES

[1]   Farzaneh, M., "Ice Accretions on High-voltage Conductors and Insulators and Related Phenomena", Philosophical Transactions of the Royal Society, Vol. 358, Nov 2000.

[2]   Farzaneh, M., Fofana, I., "Experimental Study and Analysis of Corona Discharge Parameters on an Ice Surface" J.Phys.D: Appl.Phys.37, 2004.

[3]   Zhang, J., Farzaneh, M., "Propagation of AC and DC arcs on ice surfaces", Trans. Dielectrics Electrical Insulation, 147, 2000.

[4]   Coelho R., Debeau J., "Properties of the Tip-plane Configuration", Journal of Physics: Applied Physics, Vol. 4, 1971.

[5]   Javadi, H., Farzaneh, M., "Measuring of Corona Discharge Inception Voltage to Determine Electric Field Over the Non-homogenous Electrodes in the Air Insulation", PSC2004, Tehran, 2004.

[6]   Nasser, E., "Fundamentals of gaseous ionisation and plasma electronics", J.Wiley, USA, 1971.

[7]   Abdel-Salam, M., Anis, H., El-Morshedy, A., Radwan, R., "High-Voltage Engineering, Theory and Practice", Marcel Dekker Inc.,2000.

[8]   Loeb, L.B., "Electrical Coronas, Their Basic Physical Mechanisms", 1965.

[9]   Isa, H., Sonoi, Y., Hayashi, M., "Breakdown process of a rod-to-plane gap in atmospheric air under dc voltage stress", IEEE Trans. On Electrical Insulation, Vol. 26, No. 2, April 1991.

[10] Gurumurthy, G.R., "Corona between point plane electrodes in air at atmospheric pressure", 2003 Annual Report Conference on Electrical Insulation and Dielectric Phenomena.

[11] Naidu, M.S., Kamaraju, V., "High Voltage Engineering", 1996.

[12] Hayt, W. H., Buck, J. A., "Engineering Electromagnetics", 2001.

[13] Sadiku, M.N.O., "Numerical Techniques in Electromagnetics", 2nd edition, CRS Press 2000.

[14] Kuffel, E., Zaengl, W.S., "High Voltage Engineering Fundamentals", 1992.

[15] Iravani, M.R., Raghuveer, M.R., "Accurate field solution in the entire inter-electrode space of a rod-plane gap using optimised charge simulation", IEEE Trans. On Electrical Insulation Vol. E1-17 No.4, August 1982.

[16] Kalenderli, O., Onel, E., Altay, O., "Computing the corona onset and the utilisation factor of rod-plane electrode by using charge simulation method", Electrical Insulation Conference (EIC) 2001, Cincinnati, Ohio, USA, pp. 453-456, October 16-18, 2001.

[17] Qiu, Y., "Simple expression of field non-uniformity factor for hemispherically capped rod-plane gaps", IEEE Trans. On Electrical Insulation Vol. E1-21 No.4, August 1986.

[18] Boutlendj, M., Allen, N.L., "Assessment of air-density correction for practical electrode systems", ETEP Vol. 6, No. 4, July/August 1996.

[19] Stangherlin, S., Salge, G., Koenig, F., "Measurement of discharges and their branching behaviour in atmospheric air", 2002 Annual Report Conference on Electrical Insulation and Dielectric Phenomena.

[20] IEC Publication 60060-1/1989, "High-voltage test techniques, part 1: General definitions and requirements".

[21] Allen, N.L., Kong, J., "Effect of temperature on corona onset characteristics", Proc.XIV Int. Conf. Gas Discharges & Their Applications, Liverpool, UK, 2002.

[22] Abdel-Salam, M., Allen, N.L., "Onset voltage of positive glow corona in rod-plane gaps as influenced by temperature", IEE Proc.-Sci.Meas.Technol., Vol.152, No.5, September 2005.

[23] Shu, L., Zhao, Z., Jiang, X., Tian, Z., Wang, J., "Effect of atmospheric pressure on discharge performance of short air-gaps at altitude of 4000m and above",Proc of the 7th Int. Con. On Properties and Applications of Dielectric Materials, June 1-5 2003 Nagoya.

[24] Alston, L.L., "High Voltage Technology", 1967.

[25] Cross, J. A., "Electrostatics: Principles, Problems and Applications", 1987.

[26] Hutzler, B., Hutzler, D., " Modélisation de l'amor cage des grands intervalles d'air", *Bulletin de la DER d'EDF* numéro 4,1992.

[27] Barsch, J.A., Sebo, S.A., Kolico, N., "Power frequency AC sparkover voltage measurements of small air gaps", IEEE Trans. On Power Delivery, Vol.14, No.3, July 1999.

[28] Allen, N.L., Boutlendj, M., Lightfoot, H.A., "Dielectric breakdown in non-uniform field air gaps-ranges of applicability to dc voltage measurement", IEEE Trans. On Electrical Insulation, Vol.28, No.2, April 1993.

[29] Ibrahim, O.E., "An expression for the electric field distribution in rod-plane gaps", IEEE Trans. On Electrical Insulation, Vol. 23, No. 3, June 1988.

[30] General Electric Co., Transmission Line Reference Book, "345 kV and Above", EPRI, 1982.

[31] Fofana, I., Beroual, A., "A Predictive Model of the Positive Discharge in Long Air Gaps under Pure and Oscillating Impulse Shapes", J.Phys.D: Appl.Phys.30, 1997.

[32] Borsi, H., Gockenbach, E., Schroder, U., Schiller, G., "Contribution to the Clarification of Partial Discharge Behaviour in Insulating Liquids Using the Schlieren Technique", European Transactions on Electrical Power Vol.1, No.5, September 1991.

[33] Mikropoulos, P.N., Stassinopoulos, C.A., "Atmospheric correction in rod-plane gaps up to 1m in length"IEE Proc.-Sci.Meas.Technol., 2005.

[34] Boutlendj, M., Allen, N.L., Lightfoot, H.A., Neville, R.B., "Positive DC corona and sparkover in short and long rod-plane gaps under variable humidity conditions", IEE Proc.-A, Vol.138, No 1, January 1991.

[35] Allen, N.L., Lam, D.S.K., Greaves, D.A., "Tests on the breakdown of air at elevated temperatures in non-uniform electric fields", IEE Proc.-Sci. Meas.Technol., Vol.147, No 6.November 2000.

[36] Allen, N.L., Boutlendj, M., Hughes, R.C., Lightfoot, H.A., Neville, R.B., "Analysis and comparison of rod-plane and rod-rod gaps as direct voltage measurement devices", IEE Proc.-A, Vol. 139, No. 6, November 1992.

[37] Allen, N.L., Boutlendj, M., "Study of the electric field required for streamer propagation in humid air", IEE Proc.-A, Vol. 138, No. 1, January 1991.

[38] Geldenhuys, H.J., "The Breakdown voltage of air in a 50cm rod-plane gap over a practical range of air density and humidity", The Transactions of the SA Institute of Electrical Engineers, December 1988.

[39] Schmid, J., "Influence of absolute humidity on the electrical breakdown in air", ETEP Vol. 2, No. 5, September/October 1992.

[40] Brettschneider, S., "Etudes des dimensions géométriques des glaçons réelles produit sur des isolateurs recouverts de glace", Rapport Interne, CIGÈLE, UQAC, Feb 1998.

[41] Parish, O., Putnam, T.W., "Equations for the determination of humidity from dewpoint and psychometric data", NASA Report TN-D 8401, Jan 1977.

[42] Integrated Engineering Software , Coulomb-3D Manual,Manitoba,Canada,2005.

[43] Lopez, J., Ozers, P., Judge, T.,Rebizant, C.,Bosch, R., Munoz, J., "Experience using the boundary element method in electrostatic computations as a fundamental tool in high voltage switchgear design",IEEE Transactions on Dielectric and Electrical Insulations Vol. 4, 1997.